

Manuscript Number: LITHOS7824

Title: Chromitite petrogenesis in the mantle section of the Ballantrae Ophiolite Complex (Scotland)

Article Type: Regular Article

Keywords: Ballantrae Ophiolite Complex, supra-subduction zone, podiform chromitite, upper mantle melt percolation

Corresponding Author: Dr. brian o'driscoll,

Corresponding Author's Institution:

First Author: Elizabeth J Derbyshire

Order of Authors: Elizabeth J Derbyshire; brian o'driscoll; Davide Lenaz; A Zaneti; Ralf Gertisser

Abstract: Podiform chromitites from the Ballantrae Ophiolite Complex (BOC), NW Scotland, are examined to investigate their petrogenesis and elucidate the nature of melt percolation in the supra-subduction zone oceanic mantle more generally. The mantle portion of the BOC comprises two petrologically distinct serpentinite belts, whose differences have previously been attributed to contrasting degrees of melt extraction. Chromitite occurs in each of the northern and southern serpentinite belts, at Pinbain Bridge and Poundland Burn, respectively. Field relationships suggest that chromitites were formed by melt-rock reaction in channel-like conduits in the upper mantle. Chromitite Cr-spinel compositions from the two localities show marked differences to one another, with the Pinbain Bridge chromitite Cr-spinels being characterised by relatively high Cr# [ $Cr/(Cr+Al)$ ; 0.62-0.65] and lower abundances of certain trace elements (e.g., Ti, Ga, V), whereas the Poundland Burn chromitite Cr-spinels exhibit relatively low Cr# (0.44-0.46) and higher concentrations of these trace elements. The contrasting Cr-spinel compositions are used to estimate parental magma compositions for the chromitites; the Pinbain Bridge chromitites crystallised from magmas resembling arc tholeiites whereas MORB-like magmas were involved in formation of the Poundland Burn chromitites. While it is possible that this dichotomy points to early derivation of the BOC at a MORB spreading centre, with subsequent processing in a supra-subduction zone, we suggest that the differences reflect melt extraction from different parts of an evolving subduction zone, such that the MORB-like magmas were generated in a back-arc setting. This interpretation finds support in the Ti/Fe<sup>3+</sup> versus Ga/Fe<sup>3+</sup> systematics of peridotite-hosted accessory Cr-spinel that we present here, as well as previously published trace element data and geochronological constraints on the basalt lava sequences associated with the BOC, which collectively favour formation of the Poundland Burn chromitites in subduction zone mantle.

Research Data Related to this Submission

-----  
There are no linked research data sets for this submission. The following reason is given:

Data will be made available on request



## School of Earth and Environmental Sciences

Dr Andrew Kerr,  
Editorial Board,  
Lithos

**Dr Brian O'Driscoll**  
The University of Manchester  
Williamson Building  
Oxford Road  
Manchester M13 9PL, UK

+44 (0) 1612753828  
[brian.odriscoll@manchester.ac.uk](mailto:brian.odriscoll@manchester.ac.uk)

February 27<sup>th</sup> 2019

### Re: Submission of manuscript for review in Lithos

Dear Dr Kerr,

I am submitting this cover letter on behalf of a past PhD student (co-author, Dr LJ Derbyshire), to accompany a manuscript entitled '**Chromitite petrogenesis in the mantle section of the Ballantrae Ophiolite Complex (Scotland)**'. I would be grateful if you would consider the article for publication in *Lithos*. This work has not been submitted to, accepted by, or published in any other journal.

The manuscript presents the results of a study carried out on chromitites of the lower Palaeozoic Ballantrae Ophiolite Complex (BOC), with the specific aim of using chromitite Cr-spinel compositions to elucidate the nature of melt percolation in the BOC upper mantle. Mantle Cr-spinels are relatively resistant to post-magmatic alteration (e.g., serpentinisation) so have been applied as petrogenetic indicators of their parental melt composition and degree of partial mantle melting in a variety of tectonic settings. We find that two distinct populations of chromitite are present in the BOC, mirroring previous observations that have suggested the two serpentinite belts in which the chromitites occur have experienced different melt depletion histories. The chromitite Cr-spinel compositional differences are manifest in major and trace element mineral chemistry, as well as crystal structural characteristics. Broadly speaking, the presence of the bimodal chromitite Cr-spinel compositions in the BOC permits two models for their formation. The first is a two-stage melting process that requires processing of the BOC mantle in different tectonic settings (i.e., at a mid-ocean ridge spreading centre and subsequently in a supra-subduction zone). The second explanation envisages all of the melt percolation occurring above (or associated with) an evolving subduction zone, where the population of chromitite Cr-spinels that record a lower degree of partial melting may have formed in a back-arc setting. We favour the latter scenario, for reasons that we outline in the text.

In addition to providing new insights into the petrogenesis of one of the classic UK ophiolites, we believe that our multi-technique approach to characterising chromitite Cr-spinel compositions will be of relevance to future ophiolite studies that focus on mantle petrology and subduction zone dynamics. For these reasons, we feel that this study will be of interest to the broad petrology- and mineralogy-based readership of *Lithos*.

I have taken the liberty of suggesting several referees in the dedicated section of the online submission pages, for their expertise in various aspects of ophiolite petrology, including the Ballantrae ophiolite, upper mantle processes, as well as chromitite petrogenesis, all of which are covered in this paper.

If you require any further details or information, please do not hesitate to contact me.

Yours sincerely (on behalf of all authors),



**(Brian O'Driscoll)**

---

## Chromitite petrogenesis in the mantle section of the Ballantrae Ophiolite Complex (Scotland)

Derbyshire, EJ<sup>1</sup>, O'Driscoll, B<sup>2\*</sup>, Lenaz, D<sup>3</sup>, Zanetti, A<sup>4</sup> and Gertisser, R<sup>1</sup>

<sup>1</sup>School of Geography, Geology and the Environment, Keele University, Keele, ST5 5BG, UK

<sup>2</sup>School of Earth and Environmental Sciences, University of Manchester, Oxford Road, M13 9PL, UK

<sup>3</sup>Dipartimento di Matematica e Geoscienze, Università degli Studi di Trieste, Trieste, I-34127, Italy

<sup>4</sup>Istituto di Geoscienze e Georisorse, C.N.R., Pavia, Italy

\*Corresponding author: [brian.odriscoll@manchester.ac.uk](mailto:brian.odriscoll@manchester.ac.uk)

For submission to: **Lithos**

### Abstract

Podiform chromitites from the Ballantrae Ophiolite Complex (BOC), NW Scotland, are examined to investigate their petrogenesis and elucidate the nature of melt percolation in the supra-subduction zone oceanic mantle more generally. The mantle portion of the BOC comprises two petrologically distinct serpentinite belts, whose differences have previously been attributed to contrasting degrees of melt extraction. Chromitite occurs in each of the northern and southern serpentinite belts, at Pinbain Bridge and Poundland Burn, respectively. Field relationships suggest that chromitites were formed by melt-rock reaction in channel-like conduits in the upper mantle. Chromitite Cr-spinel compositions from the two localities show marked differences to one another, with the Pinbain Bridge chromitite Cr-spinels being characterised by relatively high Cr# [ $\text{Cr}/(\text{Cr}+\text{Al})$ ; 0.62-0.65] and lower abundances of certain trace elements (e.g., Ti, Ga, V), whereas the Poundland Burn chromitite Cr-spinels exhibit relatively low Cr# (0.44-0.46) and higher concentrations of these trace elements. The contrasting Cr-spinel compositions are used to estimate parental magma compositions for the chromitites; the Pinbain Bridge chromitites crystallised from magmas resembling arc

tholeiites whereas MORB-like magmas were involved in formation of the Poundland Burn chromitites. While it is possible that this dichotomy points to early derivation of the BOC at a MORB spreading centre, with subsequent processing in a supra-subduction zone, we suggest that the differences reflect melt extraction from different parts of an evolving subduction zone, such that the MORB-like magmas were generated in a back-arc setting. This interpretation finds support in the  $Ti/Fe^{3\#}$  versus  $Ga/Fe^{3\#}$  systematics of peridotite-hosted accessory Cr-spinel that we present here, as well as previously published trace element data and geochronological constraints on the basalt lava sequences associated with the BOC, which collectively favour formation of the Poundland Burn chromitites in subduction zone mantle.

## **Chromitite petrogenesis in the mantle section of the Ballantrae Ophiolite Complex (Scotland)**

Derbyshire, EJ<sup>1</sup>, O'Driscoll, B<sup>2\*</sup>, Lenaz, D<sup>3</sup>, Zanetti, A<sup>4</sup> and Gertisser, R<sup>1</sup>

<sup>1</sup>School of Geography, Geology and the Environment, Keele University, Keele, ST5 5BG, UK

<sup>2</sup>School of Earth and Environmental Sciences, University of Manchester, Oxford Road, M13 9PL, UK

<sup>3</sup>Dipartimento di Matematica e Geoscienze, Università degli Studi di Trieste, Trieste, I-34127, Italy

<sup>4</sup>Istituto di Geoscienze e Georisorse, C.N.R., Pavia, Italy

\*Corresponding author: [brian.odriscoll@manchester.ac.uk](mailto:brian.odriscoll@manchester.ac.uk)

### **Highlights:**

- Chromitite in the Ballantrae ophiolite formed by channelized melt-rock reaction
- Significant compositional differences in chromitites from the Ballantrae ophiolite
- Calculated chromitite parental melts approximate both MORB-like and arc magmas
- Ballantrae chromitites formed during melt extraction in an evolving subduction zone

1 **Chromitite petrogenesis in the mantle section of the Ballantrae Ophiolite**  
2 **Complex (Scotland)**  
3

4 Derbyshire, EJ<sup>1</sup>, O'Driscoll, B<sup>2\*</sup>, Lenaz, D<sup>3</sup>, Zanetti, A<sup>4</sup> and Gertisser, R<sup>1</sup>

5 <sup>1</sup>School of Geography, Geology and the Environment, Keele University, Keele, ST5 5BG, UK

6 <sup>2</sup>School of Earth and Environmental Sciences, University of Manchester, Oxford Road, M13 9PL, UK

7 <sup>3</sup>Dipartimento di Matematica e Geoscienze, Università degli Studi di Trieste, Trieste, I-34127, Italy

8 <sup>4</sup>Istituto di Geoscienze e Georisorse, C.N.R., Pavia, Italy  
9  
10

11 \*Corresponding author: [brian.odriscoll@manchester.ac.uk](mailto:brian.odriscoll@manchester.ac.uk)  
12

13 For submission to: **Lithos**  
14  
15  
16

17 **Abstract**

18 Podiform chromitites from the Ballantrae Ophiolite Complex (BOC), NW Scotland, are examined  
19 to investigate their petrogenesis and elucidate the nature of melt percolation in the supra-subduction  
20 zone oceanic mantle more generally. The mantle portion of the BOC comprises two petrologically  
21 distinct serpentinite belts, whose differences have previously been attributed to contrasting degrees  
22 of melt extraction. Chromitite occurs in each of the northern and southern serpentinite belts, at  
23 Pinbain Bridge and Poundland Burn, respectively. Field relationships suggest that chromitites were  
24 formed by melt-rock reaction in channel-like conduits in the upper mantle. Chromitite Cr-spinel  
25 compositions from the two localities show marked differences to one another, with the Pinbain  
26 Bridge chromitite Cr-spinels being characterised by relatively high Cr# [ $\text{Cr}/(\text{Cr}+\text{Al})$ ; 0.62-0.65] and  
27 lower abundances of certain trace elements (e.g., Ti, Ga, V), whereas the Poundland Burn  
28 chromitite Cr-spinels exhibit relatively low Cr# (0.44-0.46) and higher concentrations of these trace  
29 elements. The contrasting Cr-spinel compositions are used to estimate parental magma  
30 compositions for the chromitites; the Pinbain Bridge chromitites crystallised from magmas  
31 resembling arc tholeiites whereas MORB-like magmas were involved in formation of the  
32 Poundland Burn chromitites. While it is possible that this dichotomy points to early derivation of



33 the BOC at a MORB spreading centre, with subsequent processing in a supra-subduction zone, we  
34 suggest that the differences reflect melt extraction from different parts of an evolving subduction  
35 zone, such that the MORB-like magmas were generated in a back-arc setting. This interpretation  
36 finds support in the  $Ti/Fe^{3\#}$  versus  $Ga/Fe^{3\#}$  systematics of peridotite-hosted accessory Cr-spinel  
37 that we present here, as well as previously published trace element data and geochronological  
38 constraints on the basalt lava sequences associated with the BOC, which collectively favour  
39 formation of the Poundland Burn chromitites in subduction zone mantle.

40

41 **Keywords:** Ballantrae Ophiolite Complex, supra-subduction zone, podiform chromitite, upper  
42 mantle melt percolation

43

## 44 **1. Introduction**

45 The harzburgitic mantle sections of some supra-subduction ophiolites preserve a rich petrological  
46 and geochemical record of melt percolation and melt-rock reaction (e.g., Boudier and Nicolas,  
47 1995; Bédard and Hébert, 1998; Piccardo et al. 2007; Rampone et al. 2008; Batanova et al., 2011;  
48 Derbyshire et al. 2013; O’Driscoll et al., 2015). The harzburgite typically hosts veins and sheets of  
49 dunite, pyroxenite and chromitite (>60 vol.% Cr-spinel) that point to a predominance of  
50 channelized, rather than porous, melt percolation in the mantle wedge (e.g., Maaløe, 2005;  
51 Batanova et al., 2011). Considerable complexity has been documented in the field relations and  
52 other characteristics of these ‘fossil’ upper mantle melt conduit systems, leading to interpretations  
53 invoking multiple generations of melt extraction. For example, O’Driscoll et al. (2015) employed  
54 Os isotopes and highly siderophile element abundances to argue that chromitites and  
55 orthopyroxenites in the ~497 Ma Leka Ophiolite Complex (Norway) formed during subduction-  
56 related melt percolation as the Iapetus Ocean closed, but that the websterites there may have formed  
57 ~80 Ma earlier, during Iapetus opening. Compositional variation in Cr-spinel in mantle peridotites  
58 and chromitites has also been utilised to elucidate a range of conditions of partial melting and melt

59 percolation in the oceanic mantle, even within the same ophiolite. Cr-spinel is relatively resistant to  
60 low temperature alteration during the serpentinisation of mantle peridotites, facilitating its  
61 widespread use as a petrogenetic fingerprinting tool, with applications in estimating the Cr-spinel  
62 parental melt composition and degree of partial mantle melting. In a study that showed how Cr-  
63 spinel chemistry could be used to decipher multiple melt extraction events, Melcher et al. (1997)  
64 reported two populations of chromitites in the Kempirsai ophiolite (Kazakhstan), one with high Cr#  
65 [Cr/(Cr+Al)] Cr-spinel and one with relatively low Cr# Cr-spinel. The low Cr# chromitites were  
66 attributed to low degree partial melting and melt percolation beneath an oceanic spreading centre  
67 (i.e., mid-ocean ridge; MOR), whilst the high Cr# chromitites were attributed to the comparatively  
68 high degrees of partial melting and fluxing of hydrous melts through a mantle wedge above a  
69 subduction zone (supra-subduction zone; SSZ). Thus, the mantle portion of the Kempirsai ophiolite  
70 was suggested to preserve evidence of ocean opening and closing, over a period of  $\geq 50$  My.

71 An increasing number of studies in recent years have recognised that podiform chromitites  
72 form by processes of melt percolation and consequent melt-rock reaction in the upper mantle (see  
73 Arai and Miura 2016 for a review). Podiform chromitites that preserve a bimodal distribution of Cr#  
74 compositions have been recorded in the mantle sections of other ophiolites, including the Semail  
75 Ophiolite (Oman; Ahmed and Arai, 2002; Rollinson, 2008), the Mayarí-Cristal Ophiolite (Cuba;  
76 González-Jiménez *et al.*, 2011), the Muğla Ophiolite (Turkey; Uysal et al., 2009) and the Luobusa  
77 Ophiolite (Tibet; Zhou *et al.*, 1996). Zhou and Robinson (1997), Ahmed and Arai (2002), Uysal et  
78 al. (2009) and Xiong et al. (2017) all invoke a model similar to that proposed by Melcher et al.  
79 (1997), whereby relatively low degrees of (anhydrous) partial melting at a MOR was followed by  
80 higher degrees of (hydrous) partial melting in a SSZ setting, forming Al- and Cr-rich chromitites,  
81 respectively. However, an alternative model proposes chromitite Cr-spinel compositions are  
82 temporally controlled by the progressive release of fluids, water and/or melt from the subducting  
83 slab during subduction zone development, forming increasingly Cr-rich chromitites over time (Zhou

84 *et al.*, 1996; Arai, 1997; Büchl *et al.*, 2004; Rollinson, 2008; González-Jiménez *et al.*, 2011;  
85 Whattam and Stern, 2011).

86 The Ballantrae Ophiolite Complex (BOC; Scotland) is a potentially useful locality to  
87 examine the extent to which the supra-subduction mantle wedge records evidence of multiple  
88 episodes of melt percolation. Firstly, geochemical studies of the lava sequences and poorly-exposed  
89 sheeted dykes have revealed broad spectrums of REE trends, ranging from LREE-enriched to  
90 LREE-depleted patterns (e.g., Wilkinson and Cann, 1974; Jones, 1977; Lewis and Bloxam, 1977;  
91 Thirlwall and Bluck, 1984; Smellie and Stone, 1992, 2001; Smellie *et al.*, 1995; Oliver and  
92 McAlpine, 1998). This led to extensive debate about the tectonic provenance of the BOC; proposed  
93 settings involve melt generation in an island arc with a back-arc basin, a MOR, a volcanic arc and  
94 the involvement of a mantle plume in the formation of the ophiolite (Wilkinson and Cann, 1974;  
95 Jones, 1977; Lewis and Bloxam, 1977; Thirlwall and Bluck, 1984; Oliver and McAlpine, 1998;  
96 Smellie and Stone, 2001). In addition, it has been suggested that the mantle portion of the BOC has  
97 been processed in different tectonic settings (Stone, 2014). In particular, the two broad serpentinite  
98 belts that comprise the BOC mantle have different petrological characteristics and sparse data  
99 published on the podiform chromitites hosted in each suggests significant differences in chromitite  
100 Cr-spinel Cr# exist (**Fig. 1**; Stone and Smellie, 1988; Stone, 2014). In this study, we present  
101 detailed new petrological and mineral chemical observations on the chromitites from the BOC. Our  
102 principal aims are to investigate the petrogenesis of chromitite in the BOC, elucidate the  
103 implications of chromitite formation for melt percolation in the palaeo-oceanic mantle preserved by  
104 the BOC, and to better constrain the conditions and setting(s) of partial mantle melting responsible  
105 for melt generation.

106

## 107 **2. Geological setting**

108 A thorough review of the different lithological components of the BOC and their contact  
109 relationships with each other has recently been published by Stone (2014). The BOC is exposed

110 over an area of  $\sim 75 \text{ km}^2$  between Girvan and Ballantrae in south-west Ayrshire, Scotland (**Fig. 1**;  
111 Bonney, 1878; Church and Gayer, 1973; Stone and Smellie, 1988). The ophiolite was obducted  
112 onto the Laurentian margin during the closure of the Iapetus Ocean (i.e., the Grampian Orogeny;  
113 Church and Gayer, 1973; Bluck et al., 1980; Oliver et al., 2002; Power and Pirrie, 2004). Obduction  
114 is dated at  $478 \pm 8 \text{ Ma}$ , by K-Ar dating of amphibolite in the ophiolite sole (Bluck et al., 1980). The  
115 complex is bound to the south by the Stinchar Valley Fault and unconformably overlain to the north  
116 by younger Llanvirn Barr and Caradoc-Ashgill Ardmillian Group sediments (Stone and Smellie,  
117 1988; **Fig. 1**). Early work by Peach and Horne (1899), Pringle (1935), Bailey and McCallien (1952,  
118 1957) and Church and Gayer (1973) attempted to explain the structural complexity of the BOC by  
119 invoking folding of the lava sequence, serpentinite intrusion and an anticlinal structure for the  
120 complex. Jones (1977) suggested that the BOC consists of a series of folded thrust sheets based on  
121 the lava sequence having uniform dips and strikes within each volcanic block, two compositionally  
122 distinct serpentinite belts and the observation that all lithological units appear to be fault-bounded.

123 The mantle portion of the BOC comprises variably serpentinitised harzburgite and dunite  
124 which crop out in two broad NE-SW trending belts (**Fig. 1**; Stone and Smellie, 1988). The northern  
125 serpentinite belt is dominantly formed of harzburgite with lherzolite and minor pyroxenite (Jelínek  
126 et al., 1980, 1984; Stone and Smellie, 1988). It is metasomatised and preserves a strong tectonic  
127 fabric. By contrast, the southern serpentinite belt comprises harzburgite with dunite, wehrlite and  
128 minor troctolite (Stone and Smellie, 1988). The southern serpentinite is less metasomatised and  
129 locally exhibits a weak tectonic fabric. Chromitite has been documented in key localities in each of  
130 the serpentinite belts, at Pinbain Bridge and at Poundland Burn (**Fig.1**; Stone and Smellie, 1988)  
131 and these are the localities that concern the present study. It has been suggested that their  
132 lithological characteristics reflect formation of the southern serpentinite belt at a shallower depth  
133 than the northern belt (Stone, 2014 and references therein). A cumulate dunite sequence (i.e., a  
134 Moho transition zone; Boudier and Nicolas, 1995) has not been clearly distinguished in the BOC.  
135 The main masses of gabbro crop out at Millenderdale and from Byne Hill to Grey Hill (**Fig. 1**). The

136 Millenderdale gabbros have been dated by K-Ar on amphibole, yielding an age of  $487 \pm 8$  Ma, and  
137 trondhjemite at Byne Hill has revealed a U-Pb zircon age of  $483 \pm 4$  Ma (Bluck et al., 1980). These  
138 gabbros exhibit intrusive relationships with their host rocks (Stone, 2014). The sheeted dyke  
139 complex in the BOC is represented at Duniewick Fort near Knockdolian, and possible poorly-  
140 developed elsewhere, e.g., at Millenderdale (**Fig. 1**; Oliver and McAlpine, 1998; Oliver et al.,  
141 2002). The basalt lava sequences are exposed to the north of the northern serpentinite belt (Pinbain,  
142 Slockenray, Brandy Craig), between the serpentinite belts (Knockormal Hill, Moak Hill, Knockdaw  
143 Hill) and to the south of the southern serpentinite belt (Mains Hill, Craig Hill, Bargain Hill; **Fig. 1**).

144

### 145 **3. Field observations at Poundland Burn and Pinbain Bridge**

146 In the northern serpentinite belt at Pinbain Bridge, a sliver of structurally-fragmented and  
147 serpentinitised harzburgite crops out in a sea cliff. The harzburgite contains small (0.2-0.5 cm; **Fig.**  
148 **2a**) brown orthopyroxene pseudomorphs and abundant serpentinite (chrysotile) veining (~5 cm  
149 thick). A pervasively serpentinitised, 4-5 m thick dunite lens occurs in the harzburgite and constitutes  
150 a broadly east-west trending zone that hosts poorly-defined lensoid chromitite bodies. The  
151 chromitite seams are characterised by variation in Cr-spinel abundance (from 60-95 vol.% Cr-  
152 spinel). Cr-spinel-rich dunites (containing 20-40 vol.% Cr-spinel) are also observed. The chromitite  
153 seams exhibit a range of thicknesses (from 5 cm to 0.5 mm). The northern margin of the chromitite  
154 band is marked by a brecciated fault zone that separates the chromitite from serpentinitised  
155 harzburgite. Both harzburgite and dunite are commonly cross-cut by abundant ~5 cm thick fibrous  
156 chrysotile veins.

157 The chromitites and Cr-spinel-bearing peridotites at Poundland Burn in the southern  
158 serpentinite belt are enclosed in dunite lenses that are interlayered with harzburgite. Harzburgite is  
159 easily distinguished from dunite by the presence of randomly-oriented, brown orthopyroxene  
160 crystals (<0.5-1 cm in size), the majority of which have been pseudomorphed by bastite.

161 Chromitites and Cr-spinel-bearing peridotites at Poundland Burn exhibit a range of textures,

162 including well-developed nodular and anti-nodular varieties (**Figs. 2b,c**). Nodular-textured  
163 chromitite is characterised by 0.2-1.5 cm diameter sub-rounded, spheroidal to ellipsoidal Cr-spinel  
164 nodules in a serpentinised dunite groundmass (**Fig. 2b**). Where the nodules are ellipsoidal, several  
165 examples exhibit weak local alignments, but most are massive-textured. Variation in nodule  
166 packing is observed. The large (>1 cm) nodules are loosely-packed with the dunite groundmass  
167 clearly distinguishable between individual nodules. However, as the Cr-spinel nodules decrease in  
168 size (from >1 to 0.2 cm), they exhibit closer-packing and a consequent decrease in groundmass  
169 proportion (i.e., from ~50 vol.% to ~25 vol.%). Smaller nodules do not tend to exhibit ellipsoidal  
170 morphologies to the same extent as the larger ones. Nodules tend to be locally very well sorted, in a  
171 given chromitite pod. However, size grading of Cr-spinel nodules from large (~1 cm) to small (<0.2  
172 cm) is observed, with the largest nodules usually in the centres of the pods. Anti-nodular chromitite  
173 is also observed, formed of a dense Cr-spinel network enclosing small (<1 cm) spheroidal or  
174 ellipsoidal volumes of serpentinised dunite (**Fig. 2c**). The Cr-spinel crystals that form the network  
175 range from <1-0.5 mm in size. Between the different nodular and anti-nodular chromitite seams, the  
176 serpentinised dunitites contain varying proportions of Cr-spinel as disseminated seams, clusters and  
177 accessory Cr-spinel crystals. For example, rounded and elongate Cr-spinel clusters of <20 crystals  
178 in dunite are formed from Cr-spinel crystals ranging from <0.2-0.5 mm in size. Small Cr-spinel  
179 stringers (<5 cm long) and thin (<1 cm) seams are also present in the dunite units. The dunitites  
180 transition to harzburgite gradationally (i.e., the boundaries between lithologies are not sharply  
181 defined) and often contain abundant magnetite veining. Harzburgite rarely contains Cr-spinel; if  
182 present, the Cr-spinel crystals occur in accessory proportions and are <0.2 cm in size.

183

#### 184 **4. Sample selection and analytical techniques**

##### 185 *4.1 Sample selection*

186

187 Sample selection was dictated to some extent by the poor degree of exposure and alteration of the

188 BOC rocks. Only chromitites (Samples BA-10-03, BA-10-04) were analysed in detail from Pinbain

189 Bridge, due to the high degrees of weathering and alteration of the peridotites there. Sample BA-10-  
190 03 is from a ~5 cm thick chromitite pod located towards the centre of the dunite lens at Pinbain  
191 Bridge, whereas BA-10-04 is from a thinner (~0.5 cm) close to the dunite-harzburgite contact. The  
192 Poundland Burn samples were collected at a poorly exposed outcrop at the head of Poundland Burn;  
193 samples of nodular chromitite (BA-10-06, BA-10-07), anti-nodular chromitite (BA-10-10), Cr-  
194 spinel-rich dunite (BA-10-13) and dunite with accessory Cr-spinel (BA-10-11, BA-10-12) were  
195 selected for further analyses. Samples BA-10-06 and BA-10-07 are nodular-textured chromitite,  
196 sampled ~2 m away from one another (along strike, in the centre of the same seam). Sample BA-  
197 10-10 is an anti-nodular chromitite sampled ~20 m away across strike from the nodular-textured  
198 chromitite that yielded BA-10-06 and BA-10-07. The relationships between BA-10-06/BA-10-07  
199 and BA-10-10 are obscured by vegetative cover. Sample BA-10-13 was collected at the margin of  
200 the nodular-textured seam, and is a Cr-spinel rich dunite with a texture somewhat resembling that of  
201 anti-nodular chromitite, but with a greater proportion of silicate present. BA-10-11 and BA-10-12  
202 are dunites from the envelope containing the main nodular-textured seam, and contain only  
203 accessory amounts of Cr-spinel.

#### 204 205 *4.2 Mineral chemistry by electron microprobe*

206 A JEOL JXA-8900RL electron microprobe at the University of Göttingen (Germany) was  
207 employed to make backscatter electron micrographs and analyse the Cr-spinel/sulfide compositions  
208 from the two target chromitite localities. Analyses were conducted on both Cr-spinel crystal cores  
209 and sieve-textured alteration rims to enable compositions of both to be studied. Cr-spinel mineral  
210 chemical data were obtained using a 20.0 kV acceleration voltage, a 20 nA beam current and a 5 µm  
211 beam diameter with a 15 s peak count and 5 s background count for Mg, Al, Cr, Fe, Si and Mn and  
212 a 30 s peak count and 15 s background count for V, Ti, Ni and Zn. The standards were MgO, Al<sub>2</sub>O<sub>3</sub>,  
213 Cr<sub>2</sub>O<sub>3</sub>, TiO<sub>2</sub>, NiO, V (synthetic), hematite for Fe, wollastonite for Si, rhodonite for Mn and gahnite  
214 for Zn. Ferric iron was calculated from the FeO content assuming perfect stoichiometry according  
215 to the method of Droop (1987). Sulphide grains situated in Cr-spinel alteration rims or adjacent to

216 Cr-spinel crystals in the serpentinitised groundmass were measured quantitatively using a 20.0 kV  
217 accelerating voltage, a 20 nA beam current and a 10  $\mu\text{m}$  beam diameter. Larger sulphide grains  
218 ( $\geq 10 \mu\text{m}$ ) were analysed with a 5  $\mu\text{m}$  beam diameter. For sulphides, peak and background count  
219 times were 15 s and 5 s, respectively, for S, Fe and Zn, 30 s and 15 s peak and background,  
220 respectively, for As, Cu, Ni, Pb, Sb, and Co and 60 s and 30 s peak and background, respectively,  
221 for Se and Te. Standards used were ZnS, AsGa, galena, gahnite and pure elements Te, Cu, Ni, Se,  
222 Sb, Fe and Co. Most sulphides were smaller than  $\sim 10 \mu\text{m}$ , so some were also analysed by EDS.

223

#### 224 *4.3 LA-ICP-MS trace elements*

225 *In situ* trace element analysis was carried out by LA-ICP-MS at IGG-CNR, Pavia (Italy), using an  
226 Elan DRC-e quadrupole mass spectrometer coupled with a Q-switched Nd-YAG laser source  
227 (Quantel Brilliant). Sample ablation was carried out with a laser beam of 266 nm wavelength and a  
228 60  $\mu\text{m}$  spot size. Helium was used as carrier gas and mixed with Ar downstream of the ablation cell.  
229 NIST SRM 610 was used as external standard, while the Al content determined by EMPA was used  
230 as the internal standard. Precision and accuracy were assessed from repeated analyses of the BCR-  
231 2g and NIST SRM 612 standards, resulting in better than  $\pm 10\%$  for concentrations at ppm levels.  
232 The LA-ICP-MS analysis was designed for the complete elemental characterisation of the spinels. It  
233 involved the concomitant acquisition of the signals of nearly 60 masses, encompassing major  
234 elements, REE, LILE, HFSE, Actinides, and most of the transitional elements relevant for the  
235 geochemical investigations. Detection limits were typically in the range of 100-500 ppb for Sc, 10-  
236 100 ppb for Sr, Zr, Ba, Gd and Pb, 1-10 ppb for Y, Nb, La, Ce, Nd, Sm, Eu, Dy, Er, Yb, Hf and Ta,  
237 and usually  $< 1$  ppb for Pr, Th and U. Further information about the analytical methods and data  
238 statistics employed is reported in Miller et al. (2012).

239 The electron microprobe Cr-spinel analyses carried out to reduce the LA-ICP-MS data were  
240 performed on a CAMECA-CAMEBAX microprobe at IGG-CNR (Istituto di Geoscienze e  
241 Georisorse-Consiglio Nazionale delle Ricerche), Padua, operating at 15 kV and 15 nA. A 20 s



242 counting time was used for both peak and total background. Synthetic  $\text{MgCr}_2\text{O}_4$  and  $\text{FeCr}_2\text{O}_4$   
243 spinels (Lenaz et al. 2004a) were used for Mg, Cr and Fe determination,  $\text{Al}_2\text{O}_3$  for Al,  $\text{MnTiO}_3$  for  
244 Ti, and Mn, NiO for Ni and sphalerite for Zn. The raw data were reduced by a PAP-type correction  
245 software provided by CAMECA.

246

#### 247 4.4 Single crystal X-ray diffraction

248 The combination of crystal structural parameters and mineral compositional data offers a potentially  
249 powerful way to evaluate Cr-spinel petrogenesis when combined with conventional mineral  
250 compositional microprobe data (cf. Lenaz et al., 2007). Eight representative Cr-spinel crystals (two  
251 from Pinbain Bridge and six from Poundland Burn) were separated from the BOC samples and  
252 analysed for their crystal structural characteristics using a KUMA-KM4 diffractometer (University  
253 of Trieste, Italy), using  $\text{MoK}\alpha$  radiation and a monochromatised graphite crystal. Twenty-four  
254 equivalent reflections (12 8 4) or (8 4 4) were used depending on the size of the Cr-spinel crystal.  
255 Structural refinements were calculated using the SHELX-97 programme (Sheldrick, 1997) using the  
256  $Fo^2_{hkl}$  in the  $Fd-3m$  space group. After X-ray data collection, the same crystals used for X-ray data  
257 collection were mounted on glass slides, polished and carbon coated for electron microprobe  
258 analyses on a CAMECA-CAMEBAX microprobe at IGG-CNR (Istituto di Geoscienze e  
259 Georisorse-Consiglio Nazionale delle Ricerche) (Padua), using the procedures and standards  
260 utilised for the Padua electron microprobe analyses described in the previous section. T and M site  
261 cation distribution was calculated using the method described in Carbonin et al. (1996) and Lavina  
262 et al. (2002). The Cr-spinel compositions obtained for crystal structural analysis at the Padova  
263 electron microprobe are consistent with the Cr-spinel compositions analysed at the University of  
264 Göttingen (Germany). Intracrystalline closure temperatures for the BOC Cr-spinel crystals were  
265 calculated using the Princivalle et al. (1999) thermometer to provide insight into compositional  
266 changes occurring during Cr-spinel crystallisation and to determine their thermal history.

267

## 268 **5. Results**

### 269 *5.1 Petrographic observations*

270 The Cr-spinel contained in the Pinbain Bridge massive-textured chromitite seams consists of  
271 subhedral to euhedral crystals that range from 50-600  $\mu\text{m}$  in size. The crystals are often highly-  
272 fractured and locally display alteration to Fe-rich thin rims around their edges, manifested by their  
273 relatively bright appearance under back-scattered electrons (**Fig. 3a**). Fine-grained magnetite is  
274 locally associated with these rims. In some instances, the rims are developed up to  $\sim 2$   $\mu\text{m}$  thick.  
275 Towards the centres of seams, Cr-spinel crystals occur as massive aggregates with poorly defined  
276 crystal boundaries. Locally, where euhedral (polygonal) crystals occur within seams, they exhibit  
277 apparent (2D) dihedral angles of  $\sim 120^\circ$  at Cr-spinel three-grain junctions, suggesting solid-state  
278 textural equilibration. The chromitite seam groundmass predominantly comprises mesh-textured  
279 serpentine pseudomorphs after olivine. Small (5-10  $\mu\text{m}$ ) irregularly-shaped sulphide grains occur in  
280 the serpentine groundmass and/or touching the altered rims at the edges of Cr-spinel crystals. More  
281 rarely, larger sulphide grains ( $>10$   $\mu\text{m}$ ) are also observed, typically touching or close to Cr-spinel  
282 crystal edges. Fractures that cut through larger (100-200  $\mu\text{m}$ ) Cr-spinels (i.e., at the centres of  
283 seams) contain abundant small ( $<20$   $\mu\text{m}$ ) Cr-spinel fragments (**Fig. 3b**). The majority of fractures  
284 that cut through Cr-spinel crystals are not associated with alteration of the Cr-spinel, suggesting  
285 they formed later, possibly in relation to the adjacent fault.

286 The Pinbain Bridge dunites hosting the chromitites are completely serpentinitised, but rare  
287 olivine pseudomorphs are present. The harzburgites are also extensively serpentinitised ( $\sim 85$ - $90$   
288 vol.%) but contain rare orthopyroxene pseudomorphs and accessory Cr-spinel ( $<1$  %). Relict  
289 olivine crystal outlines are also observed in the harzburgite, ranging in size from 0.3-0.6 mm. The  
290 pseudomorphed orthopyroxene crystals, ranging between 200-700  $\mu\text{m}$  in size, are replaced by  
291 bastite. Cr-spinel crystals (40-200  $\mu\text{m}$  in size) are anhedral and sparsely distributed throughout the  
292 fine-grained serpentine groundmass. The groundmass exhibits a mesh texture and often contains

293 thin, discontinuous veins of calcite and/or serpentine. The serpentine veins are composite, pointing  
294 towards repeated serpentinisation events.

295         The sub-rounded to elliptical chromitite nodules in the Poundland Burn chromitite seams  
296 locally display very thin and discontinuous Fe-rich alteration rims, though most nodules do not  
297 exhibit this feature at all (**Fig. 4**). Those nodules with the thickest alteration rims have irregular (i.e.,  
298 non-rounded) nodule edges. The alteration of Cr-spinel is confined to the chromitite seam edges and  
299 is almost absent from the centres of chromitite seams. A small proportion of the Cr-spinel nodules  
300 have cores that contain silicate inclusions (mostly serpentine). A typical feature of the interiors of  
301 Cr-spinel nodules is the presence of cusped-shaped areas filled with serpentine (**Figs. 3c, 4**),  
302 whereas the outer parts of nodules comprise massive Cr-spinel. Where two nodules are in contact,  
303 one may exhibit a concavity at its margin to accommodate the other, suggesting indentation. All of  
304 the nodules are moderately to heavily fractured. Cr-spinel crystals in finer grained nodular-textured  
305 seams also contain silicate inclusions (**Figs. 3c, 4a,c**). The fractures that cut through the Cr-spinel in  
306 the seams may or may not be associated with alteration of the Cr-spinel. The groundmass hosting  
307 the nodules consists of aggregates of fine-grained serpentine. Anti-nodular chromitite textures form  
308 a network of small (<100  $\mu\text{m}$ ) Cr-spinel crystals that surround (<1 mm diameter) rounded spheroids  
309 of serpentinised dunite. The Poundland Burn chromitites contain limited amounts of sulphides in  
310 the serpentinised groundmass, typically close to Cr-spinel alteration rims, or in Cr-spinel crystal  
311 fractures.

312         The Poundland Burn mantle peridotites comprise variably serpentinised harzburgite and  
313 dunite. Harzburgite contains large (<1 mm in size), randomly orientated, partially pseudomorphed  
314 orthopyroxene crystals. Where pseudomorphed, the orthopyroxene comprises bastite, mostly at the  
315 crystal edges and along cleavage planes (**Fig. 3d**). Olivine pseudomorphs, ranging from 0.2-1 mm  
316 in size, contain relict olivine domains partially replaced by a finer grained serpentine rim. The  
317 serpentinised groundmass has a reticulate texture, and rare, small (<20  $\mu\text{m}$ ) euhedral Cr-spinel  
318 crystals occur in the groundmass. The dunites contain euhedral to anhedral Cr-spinel crystals in

319 small clusters and stringers of crystals, ranging from 50-400  $\mu\text{m}$  in size (**Fig. 3e**). The abundance of  
320 Cr-spinel in dunite is variable but generally higher than in harzburgite samples. Olivine  
321 pseudomorphs are typically less than 1 mm in size and are surrounded by thin magnetite veins.  
322 Isolated Cr-spinel crystals in dunite commonly have thicker Fe-rich rims than those in the  
323 chromitites (**Fig. 3f**). Infrequently, Cr-spinel crystals contain rounded silicate inclusions in their  
324 cores, usually adjacent to fractures; this occurs in Cr-spinel crystals of all sizes, although it is  
325 generally found in larger Cr-spinels (**Fig. 3f**).

326

### 327 *5.2 Cr-spinel and sulphide major element compositions*

328 The electron microprobe analyses of the BOC chromitites (both fresh Cr-spinel cores and sieve-  
329 textured rims, as well as sulfides) are tabulated in the electronic supplement (*Table S1*). Generally,  
330 there is a marked bimodality in Cr-spinel composition between the two chromitite localities (**Fig.**  
331 **5**). Poundland Burn chromitite Cr-spinels have relatively low Cr# (0.44-0.46), similar Mg#  
332 ( $[\text{Mg}/(\text{Fe}^{2+} + \text{Mg})]$ ; 0.52-0.77) values, and higher  $\text{TiO}_2$  contents (0.21-0.27 wt.%) compared to the  
333 Pinbain Bridge chromitites overall (**Figs. 5a, 5b**). The Pinbain Bridge chromitites have moderately  
334 high Cr# (0.62-0.65), variable Mg# (0.54-0.70) and relatively low  $\text{TiO}_2$  contents (0.08-0.12 wt.%).  
335 In particular, the nodular-textured chromitites analysed from Poundland Burn have a range of Cr#  
336 (0.44-0.45), Mg# (0.70-0.77) and  $\text{TiO}_2$  (0.22-0.26 wt.%) that is distinct from the Pinbain Bridge  
337 chromitites. On plots of Cr# versus Mg# and  $\text{TiO}_2$  versus Cr# (**Fig. 5**), the Poundland Burn Cr-  
338 spinel compositions mainly fall within the abyssal peridotite or MORB fields, and the Pinbain  
339 Bridge Cr-spinels (with higher Cr# and lower  $\text{TiO}_2$ ) lie closer to (but mostly not within) the  
340 boninite field. Traverses across individual nodules in the Poundland Burn chromitite reveal that  
341 they are extremely homogenous with respect to their Cr, Al, Fe and Ti (**Fig. 4**) concentrations.  
342 Accessory Cr-spinels from Poundland Burn dunites exhibit more variable Cr# and Mg# values  
343 (0.42-0.49, 0.52-0.68, respectively) and  $\text{TiO}_2$  contents (0.21-0.36 wt.%) than the chromitite Cr-  
344 spinels (Figs. 5. The discontinuous sieve-textured alteration rims on the Pinbain Bridge Cr-spinels

345 record moderate depletion in  $Mg^{2+}$  and  $Al^{3+}$  and enrichment in  $Cr^{3+}$  and  $Fe^{3+}$  at the crystal edges, so  
346 yield values toward the higher Cr# and  $TiO_2$ , and lower Mg# end of the ranges quoted above. Thin,  
347 highly discontinuous relatively Fe-rich rims on the Cr-spinels in the Poundland Burn dunites have  
348 Cr#: 0.37-0.47 and  $TiO_2$ : 0.19-0.39 wt.%, values similar to the Fe-rich rims in the Poundland Burn  
349 chromitite Cr-spinels (Cr#: 0.38-0.54;  $TiO_2$ : 0.17-0.29 wt.%).

350 The BOC chromitites contain only sparse base-metal sulphides (and platinum-group  
351 minerals; PGM). Where present, these grains are very small ( $\sim 5 \mu m$ ) situated either in Cr-spinel  
352 crystal cores or in the serpentinised groundmass. Three small ( $< 3 \mu m$ ) Ni-Fe-S grains were  
353 identified by EDS in the serpentinised groundmass adjacent to Cr-spinel crystals in the Pinbain  
354 Bridge chromitite. One small ( $< 2 \mu m$ ) irarsite ([Ir,Ru,Rh,Pt]AsS) grain was documented at Pinbain  
355 Bridge. The nodular-textured chromitite from Poundland Burn contains several small sulphide  
356 grains ( $\sim 10 \mu m$ ) large enough for quantitative analysis. Five such sulphides were identified as  
357 heazlewoodite ( $Ni_3S_2$ ) with minor Fe impurities ( $< 1$  wt. %) and one as millerite (NiS). Other small  
358 ( $< 5 \mu m$ ) sulphides identified by EDS in the Poundland Burn chromitites include Ni-S and Ni-Fe-S  
359 grains. No PGM were analysed from any of the Poundland Burn chromitites or associated dunites.

360

### 361 5.3 Cr-spinel trace element abundances

362 All of the LA-ICP-MS data are tabulated in the electronic supplement (*Table S2*), and only those  
363 elements with particular bearing on the petrogenetic interpretation are reported below. The trace  
364 element compositional variations in the BOC chromitites mirror the major element bimodality  
365 described above. For example, the Pinbain Bridge chromitite Cr-spinels have Sc contents that range  
366 from 5.1-6.6 ppm (n=7), V from 715-865 ppm, Mn from 1265-1654 ppm, Co from 218-243 ppm  
367 and Ga from 36-43 ppm. The Poundland Burn nodular chromitite Cr-spinels have Sc contents that  
368 range from 3-5 ppm (n=8), V from 889-929 ppm, Mn from 1156-1361 ppm, Co from 223-264 ppm  
369 and Ga from 54-60 ppm. By contrast, accessory Cr-spinel in dunite from Poundland Burn has Sc  
370 contents that range from 1.3-6.2 ppm (n=6), V from 1033-1214 ppm, Mn from 1586-3071 ppm, Co

371 from 358-474 ppm and Ga from 47.6-61.7 ppm. The relationships of Ga, V and Co with Cr# are  
372 shown in **Figures 6a, 6b** and **6c**, with the fields of trace element compositions of other  
373 (unpublished) UK ophiolite Cr-spinels shown for comparison. A well-developed positive  
374 correlation is noted between Ga and Cr#, in particular (**Fig. 6a**), when considered in light of the data  
375 from other ophiolites. Values for Cu, Ni and Zn are not as easily distinguished between the different  
376 Cr-spinel groups as the aforementioned elements, though a notable positive correlation is observed  
377 between Cu/Zn versus Cu/Ni for the whole population (**Fig. 6d**), probably reflecting a sulfide  
378 control on these elements.

379 We have plotted the BOC Cr-spinel compositions on the spidergram of Pagé and Barnes  
380 (2009), which displays a range of important major and trace elements normalised to MORB (**Fig.**  
381 **7**). The Poundland Burn Cr-spinels are similar to MORB with respect to their Ga, Ti, Ni, Zn and V  
382 abundances. They are relatively enriched in Co and Mn, and depleted in Sc, compared to MORB. In  
383 contrast, the Pinbain Bridge Cr-spinels are mildly depleted in Ga and Ni, and particularly in Ti,  
384 compared to MORB. They have similar abundances of Zn, V and Sc, and are enriched in Co and  
385 Mn, relative to MORB. Compared to boninite, BOC Cr-spinels are relatively enriched in Ga, Ti and  
386 Ni, similar in terms of Zn, Co and Mn abundances, and quite depleted with respect to V and Sc.

387

#### 388 *5.4 Crystal structural measurements*

389 Cr-spinel crystals from Poundland Burn chromitites and Cr-spinel-bearing dunites have notably  
390 different cell edge lengths ( $a_0$ ) and oxygen positional parameters ( $u$ ) compared to the Cr-spinels in  
391 the Pinbain Bridge chromitites (*Table 1*, **Fig. 8**). It is worth highlighting that in spinel, the anions  
392 form a nearly cubic close-packed array, parallel to (111) planes, and the cations fill part of the  
393 tetrahedral (T) and octahedral (M) interstices available in the framework. Movement of the oxygen  
394 atom along the cube diagonal [111] causes the oxygen layers in the spinel structure to be slightly  
395 puckered so that variations in  $u$  correspond to displacements of the oxygens along the cube  
396 diagonal, and reflect adjustments to the relative effective radii of cations in the tetrahedral and

397 octahedral sites. An increase in  $u$  corresponds to an enlargement of the tetrahedral coordination  
398 polyhedra and a compensating decrease in the octahedra (Lindlsey, 1976). The Poundland Burn  
399 chromitite Cr-spinels display minimal variation in their  $a_0$  and  $u$  values (8.2204-8.2285 Å and  
400 0.2630-0.2634, respectively; **Fig. 8a**). Accessory Cr-spinel from Poundland Burn dunites displays  
401 longer cell edge lengths ( $a_0$ : 8.2456-8.2528 Å) and  $u$  values consistent with the other Poundland  
402 Burn chromitites ( $u$ : 0.2630-0.2631). Cr-spinel crystals from the Pinbain Bridge chromitites  
403 display the longest cell edge lengths ( $a_0$ : 8.2704- 8.2740 Å) and lowest  $u$  values ( $u$ : 0.2625). It is  
404 interesting to note that the Cr-spinels from Poundland Burn show the lowest cell edge lengths and  
405 the highest oxygen positional parameters among the different ophiolitic Cr-spinels analysed via X-  
406 ray single crystal diffraction (Shetland,  $a_0$ :8.26-8.31 Å;  $u$ : 0.2623-0.2631, Derbyshire et al., 2013;  
407 Oman,  $a_0$ : 8.24-8.29 Å;  $u$ : 0.2608-0.2629, Lenaz et al. 2014a; Albania,  $a_0$ : 8.27-8.31 Å;  $u$ : 0.2616-  
408 0.2627, Bosi et al., 2004; India,  $a_0$ : 8.28-8.30 Å;  $u$ : 0.2619-0.2623, Lenaz et al., 2014b).

409

## 410 **6. Discussion**

### 411 *6.1 Petrogenesis of nodular-textured and anti-nodular-textured chromitite in the BOC*

412 Podiform chromitite has been documented from the mantle portions of numerous SSZ ophiolite  
413 complexes (Dick and Bullen, 1984; Arai, 1992; Melcher et al., 1997; Barnes and Roeder, 2001;  
414 Rollinson, 2008; Pagé and Barnes, 2009; Uysal et al., 2009; González-Jiménez et al., 2010, 2011;  
415 O'Driscoll et al. 2012a; Derbyshire et al., 2013; Arai and Miura, 2016). By contrast, ophiolites that  
416 do not have a SSZ provenance do not appear to ubiquitously develop chromitite (e.g., the Lizard,  
417 UK; Taitao, Chile; see also Rollinson and Adetunji (2013) and Arai and Miura (2015) for recent  
418 discussion), suggesting that perhaps melt percolation in the supra-subduction mantle wedge is  
419 particularly conducive to their formation. The recognition that chromitite typically occurs within  
420 dunite envelopes in SSZ settings has led to widespread acceptance of melt-rock interaction  
421 mechanisms as fundamental processes for chromitite petrogenesis (Arai, 1992; 1997; Arai and  
422 Yurimoto, 1994; Zhou et al., 1996; Batanova et al., 2011; González-Jiménez et al., 2011;

423 Derbyshire et al., 2013; González-Jiménez et al., 2014a, 2014b; Arai and Miura, 2016), following  
424 the classic work of Kelemen et al. (1990) and Kelemen et al. (1992; 1995). Field observations on  
425 the BOC chromitites therefore also implicate melt-rock interaction, in ‘channels’ of focused melt  
426 flow, as the key petrogenetic mechanism. This is because chromitite bodies in the BOC are  
427 ubiquitously hosted in dunite envelopes. Where visible (e.g., at Poundland Burn), harzburgite-  
428 dunite contacts are clearly defined and relatively sharp, although gradational boundaries are also  
429 present. Dunite lenses at Pinbain Bridge and Poundland Burn invariably contain more Cr-spinel  
430 than the host harzburgite. The abundance of Cr-spinel in dunite ranges from sparse clusters and  
431 stringers oriented parallel to the dunite-harzburgite contacts, to chromitite *sensu stricto*.

432         Nodular-textured chromitite is not ubiquitous in ophiolitic mantle, but has been documented  
433 in a number of cases worldwide including the Luobusa Ophiolite (Tibet; Zhou et al., 1996, 2001),  
434 the Kempirsai Massif (Kazakhstan; Melcher et al., 1997), the Troodos Ophiolite (Cyprus;  
435 Greenbaum, 1977) and the Semail Ophiolite (Oman; Ahmed and Arai, 2002; Rollinson and  
436 Adetunji, 2013; Zagrtednov et al., 2018). Published nodular Cr-spinel analyses have been shown to  
437 display intermediate to high Cr# (0.60-0.86; Bilgrami, 1969; Greenbaum, 1977; Ahmed, 1982;  
438 Orberger et al., 1995; Vuollo et al., 1995; Zhou et al., 1996; Melcher et al., 1997; Ahmed and Arai,  
439 2002; Morishita et al., 2006; Pagé and Barnes, 2009), considerably higher than those in the BOC  
440 (Cr#: ~0.45). The formation of nodular-textured chromitite is not well understood, although most  
441 workers have implicated physical processes (Arai and Miura, 2016), e.g., the coalescence of  
442 nodules in turbulent melt flow (Lago et al., 1982), magma mixing in melt flow conduits (Ballhaus,  
443 1998) and melt-rock interaction (Zhou et al., 2001). Ballhaus (1998) showed that nodular chromitite  
444 can form by the mingling of compositionally distinct melts in melt conduits. In his experiments,  
445 Ballhaus produced nodular chromitite remarkably similar to natural examples and his model  
446 proposes that each Cr-spinel nodule forms from incomplete mixing of a silica-poor melt (from  
447 deeper in the mantle) with a more siliceous melt (produced from melting of the harzburgite host).  
448 Matveev and Ballhaus (2002) expanded the work of Ballhaus (1998) to consider the effect of water



449 on the formation of nodular chromitite, showing that the crystal-fluid and crystal-melt interfacial  
450 energies provide a control on Cr-spinel nodule formation. The Matveev and Ballhaus (2002) model  
451 proposes that fluid exsolved from a water-rich melt forms small bubbles that nucleate around  
452 dispersed Cr-spinel microphenocrysts contained within the melt. Due to the density contrast and  
453 differences in surface tension between the fluid bubbles and the melt, the Cr-spinel bearing fluid  
454 bubbles rise up the magma conduit and coalesce with other fluid bubbles to form a larger 'fluid  
455 pool' (Matveev and Ballhaus, 2002). In a more recent and novel X-ray microtomographic study,  
456 Prichard et al. (2015) reported that chromite nodules from the Troodos Ophiolite comprised a single  
457 skeletal crystal in their centres, surrounded by an outer mantle of polycrystalline chromite. The  
458 skeletal crystal at the nodule core crystallised from a chromite oversaturated melt, and Prichard et  
459 al. (2015) attributed the rounded smooth outer surfaces of nodules to dissolution by a chromite  
460 undersaturated melt. One of the main implications of the Prichard et al. (2015) Troodos study is that  
461 the random growth-by-accumulation of chromite nodules in fluid bubbles within a turbulently-  
462 flowing melt, as per the Matveev and Ballhaus model, is not necessary.

463 In the BOC, the nodular chromitites are found in close proximity to anti-nodular textured  
464 chromitite. The Cr-spinel in anti-nodular-textured chromitite has an almost identical composition  
465 (Cr#: 0.44-0.46) to that of the adjacent nodular-textured chromitite. The *in situ* growth model of  
466 Prichard et al. (2015) does not easily account for the common existence of anti-nodular chromitite.  
467 However, the BOC nodules do exhibit some textural similarities with the Troodos examples, in that  
468 silicate commonly occupies cusped areas within the interiors of nodules (**Figs. 4**), and the  
469 outer mantles of nodules comprise massive-textured Cr-spinel. Rollinson and Adetunji (2013) also  
470 described this texture in a nodule from Maqsad, in the Oman Ophiolite (see their Figure 7), so it  
471 would seem that it is a common feature of nodular-textured chromitite. However, the BOC nodules  
472 have also undergone fracturing and deformation, obscuring some of the primary microstructure and  
473 making it difficult to positively identify skeletal intergrowths at the centres of nodules (if they  
474 exist). The relative compositional homogeneity of the nodular and anti-nodular chromitites

475 combined with the lack of internal elemental zonation in individual nodules (**Fig. 4**) means that  
476 chemical evidence is not preserved for a process of magma mixing, as proposed by Ballhaus (1998).  
477 If magma mixing caused chromitite formation, then the mixing process must fortuitously have  
478 resulted in hybrid melts capable of crystallising Cr-spinel of very similar composition, despite the  
479 very different physical appearance of the nodular and anti-nodular textured chromitites. It has been  
480 noted by other studies that different chromitite textures may grade into each other, from massive  
481 textures in the centre of the chromitite pod through nodular Cr-spinel to anti-nodular and  
482 disseminated textures at the chromitite pod margin (Ahmed, 1982; Zhou et al., 1996, 2001;  
483 González-Jiménez et al., 2009, 2010; Marchesi et al., 2010; Borisova et al., 2012), suggesting a  
484 complex fluid dynamic regime. Unfortunately, a lack of exposure of the precise contact between the  
485 anti-nodular and nodular chromitites at Poundland Burn means that direct observation of the nature  
486 of the relationship between both is not possible. The nodular-textured chromitites at Poundland  
487 Burn rarely display any preferred alignment of nodules. However, indentation of nodules by one  
488 another is observed, pointing toward a degree of deformation in the conduit whilst the nodules were  
489 semi-crystalline.

490 In summary, the balance of evidence suggests that the Poundland Burn nodular chromitites  
491 formed in a conduit by melt-rock interaction, followed by a degree of flow (perhaps gravity-driven)  
492 sorting of the Cr-spinel nodules to explain the evidence for localised ductile deformation. We have  
493 not been able to verify the presence of skeletal crystals at the Cr-spinel nodule cores (cf. Prichard et  
494 al. 2015), which would point to an oversaturation event in the melt conduit. The key observation  
495 that there are cusped areas of silicate minerals within most BOC Cr-spinel nodules (**Figs. 3c, 4**)  
496 may be significant and a future research direction for the Poundland Burn chromitites will be to  
497 carry out X-ray microtomography experiments and establish whether these cusped areas are the 3D  
498 manifestations of skeletal structure in nodule interiors. The observation that size-grading of nodules  
499 occurs within individual pods of the Poundland Burn chromitites, may lend support to the Zhou et  
500 al. (2001) and Matveev and Ballhaus (2002) models of turbulent flow in melt channels. In this

501 scenario, the size range of the BOC Cr-spinel nodules (<0.2 mm to >1 cm) might be controlled by a  
502 primary physical process such as ‘snowballing’ (cf. Zhou et al., 2001). The interaction of two  
503 immiscible liquids of differing viscosities promotes turbulent flow due to the dispersion of the more  
504 vicious liquid in the less vicious fluid (Joseph et al., 1984a, 1984b; Lemenand et al., 2003; Abarzhi,  
505 2010; Abarzhi et al. 2005). The contrast between the densities and viscosities of the ascending  
506 (H<sub>2</sub>O-rich) basaltic melt (lower density and viscosity) and the siliceous melt produced from  
507 orthopyroxene dissolution in the harzburgitic host rock (higher density and viscosity) increases the  
508 Rayleigh-Taylor instability, promoting favourable conditions for turbulent flow (Huppert and  
509 Sparks, 1985; Ballhaus, 1998; Gerya and Yuen, 2003; Herbert et al., 2009; Hack and Thompson,  
510 2011). The largest (~1 cm) Cr-spinel nodules form in the centre of the melt channel where the flow  
511 is most turbulent, the melt flux is greatest and the availability of Cr is highest. The turbulent flow in  
512 the centre of the melt channel promotes the ‘snowballing’ of the developing Cr-spinel nodules,  
513 facilitating the formation of larger nodules. With increasing proximity to the channel boundary, the  
514 flow regime is more laminar, the melt flux and availability of Cr is lower, limiting the ability of the  
515 Cr-spinel nodule to ‘snowball’ and thus restricting the size of the nodules.

516         The observation of grading of Cr-spinel nodules from large (~1 cm) to small (<0.2 mm) in  
517 the Poundland Burn nodular chromitite bands can therefore be interpreted as preserving a portion of  
518 the melt channel, from the channel margin to the channel centre. As noted above, a potentially  
519 important observation that is not explained by the model above is the similar chemical composition  
520 of the nodular and anti-nodular chromitite Cr-spinels. This issue could be accounted for if magma  
521 mixing is efficient and if chromitites all formed part of the same melt channel system. The  
522 abundance of small Cr-spinel crystals surrounding the silicate nodules in the anti-nodular chromitite  
523 might suggest high Cr-spinel nucleation rates and slower crystal growth, resulting from part of the  
524 melt channel with a lower melt flux. The BOC nodular- and anti-nodular-textured chromitites have  
525 similar *u* values (0.2629-0.2634), indicating they experienced the same crystallisation and cooling  
526 history, lending indirect support to this idea.

527

528 *6.2 Petrogenetic conditions and signatures of melt percolation in the BOC mantle*

529 The compositional variation of Cr-spinel in ophiolite mantle sections has been shown to be a rich  
530 source of information on parental melt composition and the conditions of petrogenesis (cf. Dick and  
531 Bullen, 1984; Barnes and Roeder, 2001; Rollinson, 2008). In the BOC, the effects of late-stage  
532 alteration on Cr-spinel composition are relatively easy to diagnose in terms of physical appearance  
533 of crystals and compositional variation (e.g., intra-crystal fracturing, Fe-rich rims). Similarly,  
534 accessory Cr-spinels from dunites and harzburgites are not considered to retain evidence of parental  
535 melt evolution. These crystals have probably extensively reequilibrated with the dominant  
536 surrounding silicate, as shown by their higher intracrystalline closure temperatures (see below).  
537 Therefore, only those Cr-spinels considered to be free from such alteration and modification are  
538 considered in the following discussion. The distinct bimodality of Cr-spinel compositions observed  
539 between the two BOC localities is different to the continuous compositional trends observed from  
540 many SSZ ophiolite chromitites (Troodos Ophiolite, Büchl et al., 2004; Semail Ophiolite,  
541 Rollinson, 2005; and the Shetland Ophiolite Complex, Derbyshire et al., 2013), but has been  
542 documented from others as noted previously. No intermediate Cr-spinel compositions have been  
543 found in the BOC, between the relatively aluminous Cr-spinels in the Poundland Burn chromitites  
544 (Cr#: 0.44-0.46) and the Cr-rich Cr-spinels in the Pinbain Bridge chromitites (Cr#: 0.62-0.65),  
545 suggesting that these two localities reflect melt percolation under different upper mantle  
546 environmental conditions. This point is also well illustrated by consideration of where the Cr-spinel  
547 populations from Pinbain Bridge and Poundland Burn group relative to one another on of Cr#  
548 versus Mg# and TiO<sub>2</sub> versus Al<sub>2</sub>O<sub>3</sub> diagrams (**Fig. 5**). The Poundland Burn Cr-spinels plot in the  
549 MORB (abyssal peridotite) field in both instances, whereas the Pinbain Bridge Cr-spinels plot in or  
550 towards the island arc/boninite fields (**Fig. 5**).

551 The major element compositional differences between the Poundland Burn and Pinbain  
552 Bridge chromitites are also borne out in the trace element data. The Cr-spinels in the Pinbain Bridge  
553 chromitites have lower Al<sub>2</sub>O<sub>3</sub>, Ga, Ti and Ni, and generally higher Sc and Cr<sub>2</sub>O<sub>3</sub>, than the

554 Poundland Burn chromitite Cr-spinels (**Fig. 7**). The Pinbain Bridge chromitites therefore bear more  
555 resemblance to boninite Cr-spinels than the Poundland Burn chromitite Cr-spinels. Dare et al.  
556 (2009) introduced the  $Ti/Fe^{3\#}$  versus  $Ga/Fe^{3\#}$  diagram as a means of discriminating the tectonic  
557 setting and petrogenesis of Cr-spinels in mantle peridotites (**Fig. 9a**). Gallium is an interesting  
558 element for fingerprinting Cr-spinel petrogenesis because it occurs as a trivalent cation, so is  
559 unlikely to change during cooling and subsolidus processes, and is not known to be redox  
560 dependent, like  $Fe^{3+}$  (Dare et al., 2009). The diagram is principally for use with accessory Cr-  
561 spinels and there are limitations in its application to Cr-spinels from podiform chromitite, because  
562 of the important down-temperature control that host silicate plays in the chemical equilibration of  
563 Cr-spinel that is reduced or absent in chromitite. However, our dataset includes measurements of  
564 accessory dunite-hosted Cr-spinel from Poundland Burn (Samples BA-10-11, BA-10-12), that fall  
565 within the 'peridotite field' of Dare et al. (2009) on the Cr# versus Mg# diagram (**Fig. 5a**), and it is  
566 interesting to note that these spinels fall across the MOR- and SSZ-reacted field on the  $Ti/Fe^{3\#}$   
567 versus  $Ga/Fe^{3\#}$  diagram (**Fig. 9a**). The BOC chromitite analyses are included on the diagram for  
568 reference, but as noted by Dare et al. (2009), the fields they fall in may or may not reflect the  
569 petrogenetic conditions of formation. A field encompassing accessory Cr-spinels from the Lizard  
570 Ophiolite is included on **Figure 9a**, and points to a MORB setting for their crystallisation, in line  
571 with existing interpretations for that ophiolite (O'Driscoll et al., 2012b; Derbyshire, 2014).

572 The Cr-spinel crystal lattice can accommodate the substitution of cations (with different  
573 valences and ionic radii) and cation vacancies in the T and M sites (Lavina et al., 2002; Lenaz et al.,  
574 2004a, 2006; Juhin et al., 2007; Bosi et al., 2010; Fregola et al., 2011). Substitution of different  
575 cations forces the Cr-spinel crystal lattice to deform to accommodate the new cation by lattice  
576 relaxation and/or tilting of the cation sites (Juhin et al., 2007; Bosi et al., 2010; Hålenius et al.,  
577 2011). The spinel structure is non-convergent, displaying no change to the lattice symmetry  
578 between an ordered and disordered spinel (Harrison et al., 1999; Harrison and Putnis, 1999;  
579 Andreozzi et al., 2000; Nestola et al., 2007). The strong preference of  $Cr^{3+}$  for the M site can restrict

580 the exchange of Mg and Al between the T and M sites (Lenaz et al., 2004b, 2010, 2012), resulting  
581 in a more ordered spinel structure (degree of inversion (x): 0 for ordered spinel, x: 1 for disordered  
582 spinel; Andreozzi et al., 2000; Nestola et al., 2007). Sack and Ghiorso (1991) showed that a  
583 completely random cation distribution between the T and M sites has an inversion value 'x': 2/3.  
584 The low inversion values determined for the BOC Cr-spinels (x: 0.14-0.21) using the Andreozzi et  
585 al. (2000) equation shows that they have a largely ordered cation distribution. The presence of large  
586 trivalent cations in the M site (e.g., Fe<sup>3+</sup>, Cr<sup>3+</sup>) modifies the octahedral angle and shared edge  
587 resulting in a lengthening of the T-O bond (Lavina et al., 2002). Lenaz et al. (2012) suggested that if  
588 the T-O bond is longer than the M-O bond, it indicates that a large cation is situated in the T site  
589 (e.g. Fe<sup>2+</sup>). Octahedral distortion in Cr-spinel structure can be determined using the Bosi et al.  
590 (2010) equation:  $\langle\lambda_M\rangle = 1.741 - 1.301(M-O/T-O) + 0.571(M-O/T-O)^2$  with a non-distorted  
591 octahedron having  $\langle\lambda_M\rangle$ : 1. All of the BOC Cr-spinels display some distortion of the octahedron  
592 ( $\langle\lambda_M\rangle$ : 1.010-1.013), overlapping with other ophiolite Cr-spinels ( $\langle\lambda_M\rangle$ : 1.010-1.012; Bosi et al.,  
593 2004; **Fig. 8a**). The octahedral distortion in the Cr-spinel lattice directly affects the crystal stability  
594 in relation to changing parental melt composition, temperature and pressure (Bosi *et al.*, 2010). The  
595 Cr-spinel crystals from the Cr-rich Pinbain Bridge chromitites (Cr#: 0.62-0.65) have long cell edge  
596 lengths (*Table 1*), T-O bonds longer than their M-O bonds, distortion of the octahedral site and  
597 structural inversion ( $a_0$ : 8.2704-8.2740; T-O: 1.969-1.970; M-O: 1.964-1.9696;  $\langle\lambda_M\rangle$ : 1.010-1.011;  
598 x: 0.20-0.21) that is associated with a relatively ordered Cr-spinel structure resulting from the high  
599 abundance of Cr<sup>3+</sup> restricting cation exchange between the T and M sites. The Al-rich Poundland  
600 Burn Cr-spinels (Cr#: 0.44-0.46) have shorter cell edge lengths, lower structural inversion and  
601 comparable octahedral site distortion than the Pinbain Bridge Cr-spinels ( $a_0$ : 8.2204-8.528; x: 0.14-  
602 0.18;  $\langle\lambda_M\rangle$ : 1.012-1.013; *Table 1*). The T-O bond lengths in the Poundland Burn Cr-spinels  
603 correspond with Mg<sup>2+</sup> being ordered in the T site (T-O bond length for Mg<sup>2+</sup>: 1.965 Å, T-O bond  
604 length for Fe<sup>2+</sup>: 1.997 Å; Lenaz et al., 2004a). The distortion to the octahedral site in the Poundland  
605 Burn Cr-spinel crystals ( $\langle\lambda_M\rangle$ : 1.012-1.013) may not result from distortion in the tetrahedral site

606 (Bosi et al., 2010), but may be attributed to varying the extent of  $\text{Al}^{3+}$  substitution for  $\text{Cr}^{3+}$  and  $\text{Fe}^{3+}$   
607 in the M site. Therefore, the structural differences between the Cr-spinels from each locality may be  
608 a function of either compositional variation of the parental melt (controlling cation distribution by  
609 the availability and preference of  $\text{Cr}^{3+}$  for the M site; Princivalle et al., 1989; Lenaz et al., 2004b,  
610 2010, 2012), or the rate of cooling (slow cooling facilitates cation ordering between the T and M  
611 sites; Princivalle et al., 1989; Uchida et al., 2005; Lenaz et al., 2012), or a combination of both  
612 factors.

613         Crystal structural analysis of Cr-spinels can provide insights into their thermal history by  
614 utilising  $u$  values, cation ordering and by determining intracrystalline closure temperatures  
615 (Princivalle et al., 1999; Uchida et al., 2005; Lenaz et al., 2010; 2011; 2012). Intracrystalline  
616 closure temperatures calculated for the BOC Cr-spinels plot away from values previously calculated  
617 for Shetland Ophiolite Complex and Albanian Ophiolite Cr-spinels (Derbyshire et al., 2013 and  
618 Bosi et al., 2004, respectively). The Cr-spinels from the Pinbain Bridge chromitites record closure  
619 temperatures of 793-853°C. The Poundland Burn nodular-textured and anti-nodular-textured  
620 chromitites reveal crystal closure temperatures of 623-708°C and 591°C, respectively. The  
621 Poundland Burn massive-textured chromitite yields a closure temperature of 630°C, falling within  
622 the nodular chromitite temperature range. Accessory Cr-spinel in dunite from Poundland Burn  
623 yields the highest range of closure temperatures (724-789°C); this is considered to be the result of  
624 secondary ordering and/or exchange of Al and Mg cations between Cr-spinel and other mineral  
625 phases (e.g., olivine; Lenaz et al., 2011; 2012). Small  $u$  values ( $<0.2625$ ), cation disorder between  
626 the T and M sites and higher intracrystalline closure temperatures are considered to indicate rapid  
627 cooling (Princivalle et al., 1989; Della Giusta et al., 1996; Lenaz et al., 2012). Crystal structural  
628 analysis of the BOC chromitites shows that all display a limited range in  $u$  values (0.2625-0.2634), a  
629 relatively ordered structure ( $x$ : 0.14-0.21) and moderate intracrystalline closure temperatures (591-  
630 853°C). The  $u$  parameter may also be controlled by changes in the bulk chemistry of the Cr-spinel  
631 crystal (specifically  $\text{Cr}^{3+}$ ; Lenaz et al., 2007, 2010, 2011). The consistent Cr content (0.81-0.86

632 apfu) over the restricted  $u$  value range ( $u$ : 0.2629-0.2634) of the Poundland Burn Cr-spinels  
 633 indicates that changes in bulk composition have not affected the  $u$  parameter. Instead, the  $u$  values  
 634 are considered to reflect the rapid cooling of the chromitites. The correlation between lowest  $u$   
 635 values and highest Cr content ( $u$ : 0.2526-0.2625; Cr#: 0.62-0.65; **Fig. 8**, *Table 1*) in the Pinbain  
 636 Bridge Cr-spinels may result from changes to the bulk chemistry of the parental melt (increased  
 637 Cr<sup>3+</sup>) rather than from the rate of cooling.

638 We applied the algorithms of Rollinson (2008; adapted from Maurel and Maurel, 1982;  
 639 Kamenetsky et al., 2001) to calculate the chromitite parental melt Al<sub>2</sub>O<sub>3</sub> and TiO<sub>2</sub> compositions.  
 640 For the Poundland Burn chromitites (that have relatively low Cr# values), the following expressions  
 641 were applied:

$$642 \quad Al_2O_3\text{-melt} = 7.1518 \times Al_2O_3\text{-spinel}^{0.2387}$$

$$643 \quad TiO_2\text{-melt} = 1.5907 \times TiO_2\text{spinel}^{0.6322}$$

644 For the Pinbain Bridge chromitites, of likely arc affinity, the following equations were used:

$$645 \quad Al_2O_3\text{-melt} = 5.2181 \times \ln(Al_2O_3\text{-spinel}) - 1.0505$$

$$646 \quad TiO_2\text{-melt} = 1.0963 \times TiO_2\text{spinel}^{0.7863}$$

647 The calculations were only carried out for fresh Cr-spinel cores analysed from each of the BOC  
 648 chromitite localities, and reveal evidence of two compositionally distinct parental melts (**Fig. 9b**).  
 649 The Pinbain Bridge parental melt is calculated to have had 13-14 wt. % Al<sub>2</sub>O<sub>3</sub> and low TiO<sub>2</sub>  
 650 contents (~0.2 wt. %), a composition similar to that of a boninitic melt (10.0-14.4 wt. % Al<sub>2</sub>O<sub>3</sub>;  
 651 Maurel and Maurel, 1982; Kamenetsky et al., 2001; Pagé and Barnes, 2009; Uysal et al., 2009;  
 652 Derbyshire et al., 2013). The Poundland Burn chromitites (including nodular-textured chromitite)  
 653 yield higher Al<sub>2</sub>O<sub>3</sub> (16-17 wt. %) and TiO<sub>2</sub> contents (0.55-0.75 wt. %) than the Pinbain Bridge  
 654 chromitites indicating a MORB-like parental melt (MORB-like melt: >16 wt. % Al<sub>2</sub>O<sub>3</sub>). The  
 655 calculations suggest the parental melts of the accessory Cr-spinels from the Poundland Burn dunites  
 656 contained 15-16 wt. % Al<sub>2</sub>O<sub>3</sub> and 0.3-0.5 wt. % TiO<sub>2</sub>. Overall, the Poundland Burn chromitite and  
 657 Cr-spinel bearing dunite parental melts plot within the MORB field whereas the Pinbain Bridge



658 chromitite parental melts fall between the SSZ and MORB fields, suggesting formation of the latter  
659 by slightly lower degrees of partial melting than required for melts in the arc field. The presence of  
660 rare I-PGE grains (laurite [RuS<sub>2</sub>], erlichmannite [OsS<sub>2</sub>], irarsite [IrAsS] and Ir-Os-Ru alloys; Power  
661 and Pirrie, 2004) in the Pinbain Bridge chromitites and the apparent absence of PGM in the  
662 Poundland Burn chromitites provides supporting evidence for higher degrees of partial mantle  
663 melting reflected in the Pinbain Bridge Cr-spinel chemical compositions (cf. Prichard et al., 1996;  
664 Melcher et al., 1997; Ahmed and Arai, 2002; Büchl et al., 2004; González-Jiménez et al., 2011).

665

### 666 *6.3 Insights into the formation and tectonic setting of the BOC*

667 The tectonic provenance of the BOC has been the subject of protracted debate (e.g., Wilkinson and  
668 Cann, 1974; Jones, 1977; Lewis and Bloxam, 1977; Thirlwall and Bluck, 1984; Stone and Smellie,  
669 1988; Smellie and Stone, 1992, 2001; Smellie et al., 1995; Oliver and McAlpine, 1998; Stone,  
670 2014). There are multiple reasons for this, amongst the most important are the lack of good inland  
671 exposure, the structurally fragmented nature of the complex and the contrasting trace element  
672 chemistry from the different basalt lava sequences. The BOC basalt lavas have trace element  
673 compositions ranging from MORB-like (LREE-depleted; Central Balcreuchan Group 3) to island  
674 arc tholeiite-like (LREE-enriched with a negative Nb + Ta anomaly; Central Balcreuchan Group 2,  
675 Southern Balcreuchan Group 1, Southern Balcreuchan Group 2), with two further lava blocks  
676 interpreted as exhibiting ‘within-plate’ signatures (LREE-enriched with high REE concentrations;  
677 Northern Balcreuchan Group and Central Balcreuchan Group 1) (Wilkinson and Cann, 1974; Jones,  
678 1977; Thirlwall and Bluck, 1984; Smellie and Stone, 2001). In addition, boninite signatures have  
679 been documented from the Games Loup lava sequence (Stone, 2014). Previously proposed tectonic  
680 settings for the BOC have therefore included within-plate (mantle plume-related; Wilkinson and  
681 Cann, 1974), a mid-ocean ridge (Jones, 1977) and an island arc associated with a back-arc basin  
682 (Bluck et al., 1980; Thirlwall and Bluck, 1984; Smellie and Stone, 1992, 2001; Smellie et al., 1995;  
683 Oliver and McAlpine, 1998; Armstrong et al., 1999). There has been a broad general consensus

684 amongst many previous studies that the compositional disparity between the different lava blocks  
685 and gabbro units, the presence of arc-derived sediments situated beneath the lavas near Pinbain Hill  
686 (Smellie and Stone, 1992; Armstrong et al., 1999) and the MORB-like chemistry of the sheeted  
687 dyke complex (Oliver and McAlpine, 1998) point to an island arc setting with an associated back-  
688 arc basin prior to obduction of the BOC onto the Laurentian margin (Bluck et al., 1980; Thirlwall  
689 and Bluck, 1984; Smellie and Stone, 1992, 2001; Oliver and McAlpine, 1998; Armstrong et al.,  
690 1999). The formation of the back-arc basin supposedly resulted from the rifting of the Grampian  
691 arc, with the ophiolite representing the oceanward portion of the rifted arc and the back-arc basin  
692 (cf. Smellie and Stone, 1992, 2001). However, other workers have suggested alternating  
693 obduction/accretion events with basin filling and volcanism (Bluck, 1990; 2002).

694         The mantle portions of the BOC, as represented by the northern and southern serpentinite  
695 belts, are lithologically and chemically distinct from one another and therefore also contribute to the  
696 difficulty in invoking a single tectonic environment of formation for the BOC. The northern  
697 serpentinite contains a lithological assemblage and other characteristics consistent with it  
698 representing more depleted oceanic mantle than that preserved in the southern serpentinite belt  
699 (Stone, 2014). The Cr-spinel data reported here serve to further highlight the distinction between the  
700 two serpentinite belts. Indeed, the Cr# of chromitite Cr-spinel can be used to estimate the degree of  
701 partial mantle melting in each serpentinite (after Hellebrand et al., 2001; Chapter 2). The  
702 relationship put forward in Hellebrand et al. (2001) is:

$$703 \qquad F = 10\ln(\text{Cr}\#) + 24$$

704 where F is the degree of partial mantle melting. The equation is derived from the correlation of  
705 HREE (specifically Dy, Er and Yb) in clinopyroxene with the Cr# of Cr-spinel and is calibrated for  
706 Cr-spinels with Cr#: 0.10-0.60, a range which covers the majority of abyssal Cr-spinel  
707 compositions. Voigt and von der Handt (2011) determined that for Cr-spinels with Cr#: >0.60, the  
708 equation underestimates the degree of mantle partial melting. The Poundland Burn chromitites and  
709 Cr-spinel-bearing dunites yield a range of F of 14-16% partial melting, with the dunites consistently

710 giving 1% higher (~16%) degrees of partial melting than the chromitites (14-15%). The Pinbain  
711 Bridge chromitites reveal values in the range 19-20% but as noted above this is likely to be an  
712 underestimate as these Cr-spinels have typical Cr# values in the range 0.62-0.65. Notwithstanding  
713 this uncertainty, the comparatively lower degree of partial melting calculated from the Poundland  
714 Burn chromitites lends support to the notion that these formed in less refractory mantle than the  
715 Pinbain Bridge chromitites.

716 Broadly speaking, the presence of the bimodal chromitite compositions in the BOC permits  
717 at least two models for their formation. The first is a two-stage melting process that requires  
718 processing of the BOC mantle in different tectonic settings (i.e., MOR and SSZ; cf., Melcher et al.,  
719 1997; Ahmed and Arai, 2002; Uysal et al., 2009). The second explanation envisages all of the melt  
720 percolation occurring above (or associated with) a developing subduction zone. In the latter case, it  
721 is possible that low Cr# chromitite could develop with incipient fore-arc (low degree) partial  
722 melting, with progression to higher Cr# chromitite as hydrous fluxing of the mantle wedge  
723 developed properly, analogous to the 'subduction initiation' geochemical evolution of ophiolite lava  
724 sequences proposed by Whattam and Stern (2011). Another option is that the low Cr# chromitite  
725 reflects melt percolation in the mantle below a back-arc spreading centre, simulating MORB-like  
726 melt depletion, which would necessarily be coeval with or postdate the high Cr# chromitite  
727 formation. Although imprecise, the chronological information available for the BOC points to the  
728 latter as being the more likely scenario. This is because the available geochronology (see Stone  
729 2014 for a summary) points to a significant temporal overlap between the arc and 'within-plate'  
730 lava sequences in the BOC. Whether fore-arc or back-arc, the characteristics of the Poundland Burn  
731 peridotite Cr-spinels on the Ti/Fe<sup>3</sup># versus Ga/Fe<sup>3</sup># diagram of Dare et al. (2009; **Fig. 9a**) also  
732 support a subduction-related environment of formation for the dunite (and therefore the chromitite)  
733 channels, rather than a MORB setting.

734 One of the lines of support for melt generation in a back-arc setting comes from the presence  
735 of LREE-enriched lavas with high Zr/Nb, low Zr/Y ratios and high REE concentrations (Northern

736 Balcreuchan Group at Pinbain, Slockenray, Brandy Craig and the Central Balcreuchan Group at  
737 Bennane Head). The Northern Balcreuchan Group and Central Balcreuchan Group 1 lavas display  
738 enrichment in the HFSE and REE and do not exhibit a negative Nb + Ta anomaly (Thirlwall and  
739 Bluck, 1984; Smellie and Stone, 2001). Interestingly, the apparent absence of a Nb depletion  
740 signature in some arc lavas and tuffs from the Aeolian arc (southern Italy), the Aegean arc (Greece)  
741 and in western Ireland as observed, for example, by Clift and Blusztajn (1999) and Draut and Clift  
742 (2001), has been attributed to the slowing and termination of subduction. The LREE-enriched  
743 Northern Balcreuchan Group and Central Balcreuchan Group 1 lavas might therefore represent late-  
744 stage melts formed during the slowing and eventual termination of the southward subduction before  
745 the subduction polarity reversal after the accretion of the Grampian arc (Dewey and Ryan, 1990;  
746 Ryan and Dewey, 1991; Oliver et al., 2002; Strachan et al., 2002; Dewey, 2005; MacDonald and  
747 Fettes, 2006). The slowing of subduction would restrict the amount of fluid available for fluxing the  
748 mantle wedge thus lowering the degree of partial melting. The resulting melt would be enriched in  
749 LILE, HFSE and LREE, but would also generate chromitite with lower Cr#, offering a plausible  
750 scenario for the petrogenesis of the Poundland Burn chromitites forming in the mantle beneath a  
751 back-arc spreading centre.

752

## 753 **7. Summary and Conclusions**

754 Although obscured to a degree by late-stage faulting and secondary alteration (serpentinisation), the  
755 Ballantrae Ophiolite Complex preserves evidence for melt extraction and percolation in a SSZ  
756 environment. The Pinbain Bridge and Poundland Burn chromitites formed by melt-rock reaction in  
757 channel-like conduits in the upper mantle. Although the formation of nodular-textured chromitite in  
758 ophiolitic mantle is generally not well understood (Arai and Miura, 2016), the BOC examples have  
759 textural and lithological similarities to those reported from other ophiolites (including Oman and  
760 Troodos). This suggests a common mechanism of formation and, looking forward, new constraints  
761 on their petrogenesis may result from the application of the X-ray microtomography technique of  
762 Prichard et al. (2015) to test for an origin by *in situ* crystallisation. The petrological differences

763 previously documented between the northern and southern serpentinite limbs of the BOC are  
764 reflected in the chemical compositions of chromitite Cr-spinel from each.

765         The presence of high-Cr# (Pinbain Bridge) and low Cr# (Poundland Burn) chromitites  
766 suggests that either the Ballantrae mantle section preserves evidence for melt extraction at both a  
767 MOR and in a SSZ setting, or the contrasting chromitite compositions reflect progressive changes in  
768 the compositions of the parental melts (and hence the style of melt extraction) in a complex  
769 subduction zone setting. Our combined datasets and observations suggest that the latter scenario is  
770 more likely, and the trace element characteristics of accessory Cr-spinel formed in dunite at  
771 Poundland Burn (i.e., illustrated in **Fig. 9a**) serve to support this inference. Given the diversity of  
772 basalt compositions associated with the BOC (cf. Stone, 2014), the contrasting signatures preserved  
773 in the chromitites provide a useful dimension to aiding interpretation of the environment of  
774 formation of the ophiolite, as well as highlighting more generally the utility of mantle-hosted  
775 chromitites as for finger-printing melt percolation and melt-rock reaction.

776

## 777 **Acknowledgements**

778

779 The work in this paper forms part of the PhD research carried out by EJ Derbyshire at Keele  
780 University (Derbyshire, 2014). Funding for the work presented in this article was received by EJD  
781 from the Edinburgh Geological Society, the EPSAM Research Institute (Keele University) and the  
782 Keele Postgraduate Association (Keele University) and is gratefully acknowledged. Funding for the  
783 trace element analysis of Cr-spinels was provided to DL by the University of Trieste (FRA2009).  
784 B.O'D. acknowledges support from a Royal Society Research Grant (RG100528) and from Natural  
785 Environment Research Council (NERC) New Investigator grant NE/J00457X/1 whilst based at  
786 Keele University. Peter Greatbatch and Dave Wilde are acknowledged for their excellent thin-  
787 section production.

788

789

790

791

792

## 793 **References**

794

795 Abarzhi, S., 2010. On fundamentals of Rayleigh-Taylor turbulent mixing. *EPL (Europhysics*  
796 *Letters)* 91(3), 35001.

797

798 Abarzhi, S., Gorobets, A. and Sreenivasan, KR., 2005. Rayleigh-Taylor turbulent mixing of  
799 immiscible, miscible and stratified fluids. *Physics of Fluids* 17(8), 081705.

800

801 Ahmed, Z., 1982. Prophyritic-nodular, nodular and orbicular chrome ores from the Sakhakot-Qila  
802 complex Pakistan, and their chemical variations. *Mineralogical Magazine* 45, 167-178.  
803  
804 Ahmed, A. H., Arai, S., 2002. Unexpectedly high-PGE chromitite from the deeper mantle section of  
805 the northern Oman ophiolite and its tectonic implications. *Contributions to Mineralogy and*  
806 *Petrology* 143, 263-278.  
807  
808 Andreozzi, G. B., Princivalle, F., Skogby, H., Della Giusta, A., 2000. Cation ordering and structural  
809 variation with temperature in MgAl<sub>2</sub>O<sub>4</sub> spinel: an X-ray single crystal study. *American*  
810 *Mineralogist* 85, 1164-1171.  
811  
812 Arai, S., 1992. Chemistry of chromian spinel in volcanic rocks as a potential guide to magma  
813 chemistry. *Mineralogical Magazine* 56, 173-184.  
814  
815 Arai, S., 1997. Control of wall-rock composition on the formation of podiform chromitites as a  
816 result of magma/peridotite interaction. *Resource Geology* 47, 177-187.  
817  
818 Arai, S., Yurimoto, H., 1994. Podiform chromitites of the Tari-Misaka Ultramafic Complex,  
819 Southern Japan, as mantle-melt interaction products. *Economic Geology* 89, 1279-1288.  
820  
821 Arai, S., Miura, M., 2015. Podiform chromitites do form beneath mid-ocean ridges. *Lithos* 232,  
822 143-149.  
823  
824 Arai, S. and Miura, M., 2016. Formation and modification of chromitites in the mantle. *Lithos* 264,  
825 277-295.  
826  
827 Armstrong, H. A., Owen, A. W., Floyd, J. D., 1999. Rare earth geochemistry of Arenig cherts from  
828 the Ballantrae Ophiolite and Leadhills Imbricate Zone, southern Scotland: implications for origin  
829 and significance to the Caledonian orogeny. *Journal of the Geological Society* 156, 549-560.  
830  
831 Bailey, E. B., McCallien, W. J., 1952. Ballantrae problems: a historical review. *Transactions of the*  
832 *Edinburgh Geological Society* 15, 14-38.  
833  
834 Bailey, E. B., McCallien, W. J., 1957. The Ballantrae Serpentine, Ayrshire. *Transactions of the*  
835 *Edinburgh Geological Society* 17, 33-53.  
836  
837 Ballhaus, C., 1998. Origin of podiform chromite deposits by magma mingling. *Earth and Planetary*  
838 *Science Letters* 156, 185-193.  
839  
840 Barnes, S. J., Roeder, P., 2001. The range of spinel compositions in terrestrial mafic and ultramafic  
841 rocks. *Journal of Petrology* 42, 2279-2302.  
842  
843 Batanova, V. G., Belousov, I. A., Savelieva, G. N., Sobolev, A. V., 2011. Consequences of  
844 channelized and diffuse melt transport in supra-subduction zone mantle: Evidence from the Voykar  
845 Ophiolite (Polar Urals). *Journal of Petrology* 52, 2483-2521.  
846  
847 Bédard, J. H., Hébert, R., 1998. Formation of chromitites by assimilation of crustal pyroxenites and  
848 gabbros into peridotitic intrusions: North Arm Mountain Massif, Bay of Islands ophiolite,  
849 Newfoundland, Canada. *Journal of Geophysical Research* 103(B3), 5165-5184.  
850  
851 Bilgrami, S. A., 1969. Geology and chemical mineralogy of the Zhob Valley chromite deposits,  
852 west Pakistan. *The American Mineralogist* 54, 134-148.

853  
854 Bluck, B. J., 1990. Terrane provenance and amalgamation: examples from the Caledonides.  
855 Philosophical Transactions of the Royal Society of London, Series A, Mathematical and Physical  
856 Sciences 331, 599-609.  
857  
858 Bluck, B. J., 2002. The midland Valley terrane, in: Trewin, N. H. (Ed.), The Geology of Scotland  
859 (2nd Edition). The Geological Society, London, pp. 167-200.  
860  
861 Bluck, B. J., Halliday, A. N., Aftalion, M., MacIntyre, R. M., 1980. Age and origin of Ballantrae  
862 ophiolite and its significance to the Caledonian Orogeny and Ordovician time scale. *Geology* 8,  
863 492-495.  
864  
865 Bonney, T. G., 1878. On the serpentine and associated igneous rocks of the Ayrshire coast.  
866 *Quarterly Journal of the Geological Society* 34, 769-785.  
867  
868 Borisova, A. Y., Ceuleneer, G., Kamenetsky, V. S., Arai, S., Bénjina, F., Abily, B., Bindeman, I.  
869 N., Polvé, M., de Parseval, P., Aigouy, T., Pokrovski, G. S., 2012. A new view on the petrogenesis  
870 of the Oman Ophiolite chromitites from microanalyses of chromite-hosted inclusions. *Journal of*  
871 *Petrology* 53, 2411-2440.  
872  
873 Bosi, F., Andreozzi, G., Ferrini, V., Lucchesi, S., 2004. Behaviour of cation vacancy in  
874 kenotetrahedral Cr-spinels from Albanian eastern belt ophiolites. *American Mineralogist* 89, 1367–  
875 1373.  
876  
877 Bosi, F., Hålenius, U., Skogby, H., 2010. Crystal chemistry of the MgAl<sub>2</sub>O<sub>4</sub>-MgMn<sub>2</sub>O<sub>4</sub>-  
878 MnMn<sub>2</sub>O<sub>4</sub> system: analysis of structural distortion in spinel- and hausmannite-type structures.  
879 *American Mineralogist* 95, 602-607.  
880  
881 Boudier, F., Nicolas, A., 1995. Nature of the Moho Transition Zone in the Oman Ophiolite. *Journal*  
882 *of Petrology* 36, 777-796.  
883  
884 Büchl, A., Brüggemann, G. E., Batanova, V. G., 2004. Formation of podiform chromitite deposits:  
885 implications from PGE abundances and Os isotopic compositions of chromites from the Troodos  
886 complex, Cyprus. *Chemical Geology* 208, 217-232.  
887  
888 Carbonin, S., Russo, U., Della Giusta, A., 1996. Cation distribution in some natural spinels from X-  
889 ray diffraction and Mössbauer spectroscopy. *Mineralogical Magazine* 60, 355-368.  
890  
891 Church, W. R., Gayer, R. A., 1973. The Ballantrae Ophiolite. *Geological Magazine* 110, 497-510.  
892  
893 Clift, P., Blusztajn, J., 1999. The trace-element characteristics of Aegean and Aeolian volcanic arc  
894 marine tephra. *Journal of Volcanology and Geothermal Research* 92, 321-347.  
895  
896 Dare, S. A. S., Pearce, J. A., McDonald, I., Styles, M. T., 2009. Tectonic discrimination of  
897 peridotites using fO<sub>2</sub>-Cr# and Ga-Ti-Fe<sup>III</sup> systematics in chrome-spinel. *Chemical Geology* 261,  
898 199–216.  
899  
900 Della Giusta, A., Carbonin, S., Ottonello, G., 1996. Temperature-dependent disorder in a natural  
901 Mg-Al-Fe<sup>2+</sup>-Fe<sup>3+</sup>-spinel. *Mineralogical Magazine* 60, 603-616.  
902  
903 Derbyshire, E. J., 2014. Upper mantle processes, serpentinisation and late-stage alteration preserved  
904 in British ophiolite peridotites and chromitites. PhD Thesis, Keele University, UK, 236 pp

905  
906 Derbyshire, E.J., O'Driscoll, B., Lenaz, D., Gertisser, R., Kronz, A., 2013. Compositionally  
907 heterogeneous podiform chromitite in the Shetland Ophiolite Complex (Scotland): implications for  
908 chromitite petrogenesis and late-stage alteration in the upper mantle portion of a supra-subduction  
909 zone ophiolite. *Lithos*, 162-163, 279-300.  
910  
911 Dewey, J. F., 2005. Orogeny can be very short. *Proceedings of the National Academy of Sciences*  
912 of the United States of America 102, 15286-15293.  
913  
914 Dewey, J. F., Ryan, P. D., 1990. The Ordovician evolution of the South Mayo trough, western  
915 Ireland. *Tectonics* 9, 887-902.  
916  
917 Dick, H. J. B., Bullen, T., 1984. Chromium-spinel as a petrogenetic indicator in abyssal and alpine-  
918 type peridotites and spatially associated lavas. *Contributions to Mineral Petrology* 86, 54-76.  
919  
920 Draut, A. E., Clift, P. D., 2001. Geochemical evolution of arc magmatism during arc continent  
921 collision, South Mayo, Ireland. *Geology* 29, 543-546.  
922  
923 Droop, G. T. R., 1987. A general equation for estimating Fe<sup>3+</sup> concentrations in ferromagnesian  
924 silicates and oxides from microprobe analyses, using stoichiometric criteria. *Mineralogical*  
925 *Magazine* 51, 431-435.  
926  
927 Fregola, R. A., Bosi, F., Skogby, H., 2011. A first report on anion vacancies in a defect MgAl<sub>2</sub>O<sub>4</sub>  
928 natural spinel. *Periodico di Mineralogia* 80, 27-38.  
929  
930 Gerya, T. V., Yuen, D. A., 2003. Rayleigh-Taylor instabilities from hydration and melting propel  
931 'cold plumes' at subduction zone. *Earth and Planetary Science Letters* 212, 47-62.  
932  
933 González-Jiménez, J. M., Kerestedjian, T., Proenza, J. A., Gervilla, F., 2009. Metamorphism on  
934 chromite ores from the Dobromirski Ultramafic Massif, Rhodope Mountains (SE Bulgaria).  
935 *Geologica Acta* 7, 413-429.  
936  
937 González-Jiménez, J. M., Gervilla, F., Kerestedjian, T., Proenza, J. A., 2010. Alteration of  
938 Platinum-group and Base-Metal mineral assemblages in ophiolite chromitites from the Dobromirski  
939 Massif, Rhodope Mountains (Bulgaria). *Resource Geology* 60, 315-334.  
940  
941 González-Jiménez, J. M., Proenza, J. A., Gervilla, F., Melgarejo, J. C., Blanco-Moreno, J. A., Ruiz-  
942 Sanchez, R., Griffin, W. L., 2011. High-Cr and high-Al chromitites from the Sagua de Tánamo  
943 district, Mayarí-Cristal ophiolitic massif (eastern Cuba): Constraints on their origin from  
944 mineralogy and geochemistry of chromian spinel and platinum-group elements. *Lithos* 125, 101  
945 121.  
946  
947 González-Jiménez, J.M., Griffin, W.L., Gervilla, F., Proenza, J.A., O'Reilly, S.Y., Pearson, N.J.,  
948 2014a. Chromitites in ophiolites: how, where, when, why? Part I. Origin and significance of  
949 platinum-group minerals. *Lithos* 189, 127-139  
950  
951 González-Jiménez, J.M., Griffin, W.L., Proenza, J.A., Gervilla, F., O'Reilly, S.Y., Akbulut, M.,  
952 Pearson, N.J., Arai, S., 2014b. Chromitites in ophiolites: how, where, when, why? Part II. The  
953 crystallisation of chromitites. *Lithos* 189, 140-158  
954  
955 Greenbaum, D., 1977. The chromitiferous rocks of the Troodos Ophiolite Complex, Cyprus.  
956 *Economic Geology* 72, 1175-1194.



957  
958 Hack, A. C., Thompson, A. B., 2011. Density and viscosity of hydrous magmas and related fluids  
959 and their role in subduction zone processes. *Journal of Petrology* 52, 1333-1362.  
960  
961 Hålenius, U., Bosi, F., Skogby, H., 2011. A first record of strong structural relaxation of TO4  
962 tetrahedra in a spinel solid solution. *American Mineralogist* 96, 617-622.  
963  
964 Harrison, R. J., Putnis, A., 1999. Determination of the mechanism of cation ordering in  
965 magnesioferrite (MgFe<sub>2</sub>O<sub>4</sub>) from the time- and temperature-dependence of magnetic susceptibility.  
966 *Physics and Chemistry of Minerals* 26, 322-332.  
967  
968 Harrison, R. J., Dove, M. T., Knight, K. S., Putnis, A., 1999. In-situ neutron diffraction study of  
969 non-convergent cation ordering in the (Fe<sub>3</sub>O<sub>4</sub>)<sub>1-x</sub>(MgAl<sub>2</sub>O<sub>4</sub>)<sub>x</sub> spinel solid solution. *American*  
970 *Mineralogist* 84, 555-563.  
971  
972 Hellebrand, E., Snow, J. E., Dick, H. J. B., Hofmann, A. W., 2001. Coupled major and trace  
973 elements as indicators of the extent of melting in mid-ocean ridge peridotites. *Nature*, 410, 677-681.  
974  
975 Herbert, L. B., Antoshechkina, P., Asimow, P., Gurnis, M., 2009. Emergence of a low viscosity  
976 channel in subduction zones through the coupling of mantle flow and thermodynamics. *Earth and*  
977 *Planetary Science Letters* 278, 243-256.  
978  
979 Hunt, E., O'Driscoll, B., Daly, J.S., 2012. Parental magma composition of the syn-tectonic Dawros  
980 Peridotite chromitites, NW Connemara, Ireland. *Geological Magazine*, 149(4), 590-605.  
981  
982 Huppert, H. E., Sparks, R. S. J., 1985. Cooling and contamination of mafic and ultramafic magmas  
983 during ascent through continental crust. *Earth and Planetary Science Letters* 74, 371-386.  
984  
985 Jelínek, E., Soucek, J., Bluck, B. J., Bowes, D. R., Treloar, P. J., 1980. Nature and significance of  
986 beerbachites in the Ballantrae ophiolite, SW Scotland. *Transactions of the Royal Society of*  
987 *Edinburgh: Earth Sciences* 71, 159-179.  
988  
989 Jelínek, E., Soucek, J., Randa, Z., Jakeš, P., Bluck, B. J., Bowes, D. R., 1984. Geochemistry of  
990 peridotites, gabbros and trondhjemites of the Ballantrae complex, SW Scotland. *Transactions of the*  
991 *Royal Society of Edinburgh: Earth Sciences* 75, 193-209.  
992  
993 Jones, C. M., 1977. The Ballantrae Complex as compared to the ophiolites of Newfoundland.  
994 Unpublished Ph. D thesis, Cardiff University.  
995  
996 Joseph, D. D., Renardy, M., Renardy, Y., 1984a. Instability of the flow of two immiscible liquids  
997 with different viscosities in a pipe. *Journal of Fluid Mechanics* 141, 309- 317.  
998  
999 Joseph, D. D., Nguyen, K., Beavers, G. S., 1984b. Non-uniqueness and stability of the  
1000 configuration of flow of immiscible fluids with different viscosities. *Journal of Fluid Mechanics*  
1001 141, 319-345.  
1002  
1003 Juhin, A., Calas, G., Cabaret, D., Galois, L., Hazemann, J-L., 2007. Structural relaxation around  
1004 substitutional Cr<sup>3+</sup> in MgAl<sub>2</sub>O<sub>4</sub>. *Physical Review B* 76, doi:10.1103/PhysRevB.76.054105  
1005  
1006 Kamenetsky, V. S., Crawford, A. J., Meffre, S., 2001. Factors controlling chemistry of magmatic  
1007 spinel: an empirical study of associated olivine, Cr-spinel and melt inclusions from primitive rocks.  
1008 *Journal of Petrology* 42, 655–671.

1009  
1010 Kelemen, P. B., Johnson, K. T. M., Kinzler, R. J., Irving, A. J., 1990. High-field-strength element  
1011 depletions in arc basalts due to mantle-magma interaction. *Nature* 345, 521-524.  
1012  
1013 Kelemen, P. B., Dick, H. J. B., Quick, J. E., 1992. Formation of harzburgite by pervasive melt/rock  
1014 interaction in the upper mantle. *Nature* 358, 365-641.  
1015  
1016 Kelemen, P. B., Shimizu, N., Salters, V. J. M., 1995. Extraction of mid-ocean ridge basalt from the  
1017 upwelling mantle by focused flow of melt in dunite channels. *Nature* 375, 747-753.  
1018  
1019 Kepezhinskas, P. K., Taylor, R. N. & Tanaka, H., 1993. Geochemistry of plutonic spinels from the  
1020 north Kamchatka arc: comparisons with spinels from other tectonic settings. *Mineralogy Magazine*  
1021 57, 575-589.  
1022  
1023 Kovács, G. P., Buda, G., Watkinson, D. H., Tompa, L., 1997. Chromite deposits of the Sagua-  
1024 Baracoa range, Eastern Cuba. *Acta Geologica Hungarica* 40, 337-353.  
1025  
1026 Lago, B. L., Rabinowicz, M., Nicolas, A., 1982. Podiform chromite ore bodies: a genetic model.  
1027 *Journal of Petrology* 23, 103-125.  
1028  
1029 Lavina, B., Salviulo, G., Della Guista, A., 2002. Cation distribution and structural modelling of  
1030 spinel solid solutions. *Physics and Chemistry of Minerals* 29, 10-18.  
1031  
1032 Lemenand, T., Della Valle, D., Zellouf, Y., Peerhossaini, H., 2003. Droplets formation in turbulent  
1033 mixing of two immiscible fluids in a new type of static mixer. *International Journal of Multiphase*  
1034 *Flow* 29, 813-840.  
1035  
1036 Lenaz, D., Skogby, H., Princivalle, F., Hålenius, U., 2004a. Structural changes and valence states  
1037 in the  $MgCr_2O_4 - FeCr_2O_4$  solid solution series. *Physics and Chemistry of Minerals* 31, 633-642.  
1038  
1039 Lenaz, D., Andreozzi, G. B., Mitra, S., Bidyananda, M., Princivalle, F., 2004b. Crystal chemical  
1040 and  $^{57}Fe$  Mössbauer study of chromite from the Nuggihalli schist belt (India). *Mineralogy and*  
1041 *Petrology* 80, 45-57.  
1042  
1043 Lenaz, D., Skogby, H., Princivalle, F., Hålenius, U., 2006. The  $MgCr_2O_4-MgFe_2O_4$  solid solution  
1044 series: effects of octahedrally coordinated  $Fe^{3+}$  on T-O bond lengths, *Physics and Chemistry of*  
1045 *Minerals* 33, 465-474.  
1046  
1047 Lenaz, D., Braidotti, R., Princivalle, F., Garuti, G., Zaccarini, F., 2007. Crystal chemistry and  
1048 structural refinements of chromites from different chromitite layers and xenoliths of the Bushveld  
1049 Complex. *European Journal of Mineralogy* 19, 599-609.  
1050  
1051 Lenaz, D., De Min, A., Garuti, G., Zaccarini, F., Princivalle, F., 2010. Crystal chemistry of Cr-  
1052 spinels from the lherzolite mantle peridotite of Ronda (Spain). *American Mineralogist* 95, 1323-  
1053 1328.  
1054  
1055 Lenaz, D., O'Driscoll, B., Princivalle, F., 2011. Petrogenesis of the anorthosite-chromitite  
1056 association: crystal-chemical and petrological insights from the Rum Layered Suite, NW Scotland.  
1057 *Contributions to Mineralogy and Petrology* 162, 1201-1213.  
1058

- 1059 Lenaz, D., Garuti, G., Zaccarini, F., Cooper, R. W., Princivalle, F., 2012. The Stillwater Complex  
1060 chromitites: the response of chromite crystal chemistry to magma injection. *Geologica Acta* 10, 33-  
1061 41.  
1062
- 1063 Lenaz, D., Adetunji, J., Rollinson, H., 2014a. Determination of  $Fe^{3+}/\Sigma Fe$  ratios in chrome spinels  
1064 using a combined Mössbauer and single-crystal X-ray approach: application to chromitites from the  
1065 mantle section of the Oman ophiolite. *Contributions to Mineralogy and Petrology* 167, article 958.  
1066
- 1067 Lenaz, D., Andreozzi, G.B., Bidyananda, M., Princivalle, F., 2014b. Oxidation degree of chromite  
1068 from Indian ophiolites: a crystal chemical and  $^{57}Fe$  Mössbauer study. *Periodico di Mineralogia* 83,  
1069 241-255,  
1070
- 1071 Lewis, A. D., Bloxam, T. W., 1977. Petrotectonic environments of the Girvan-Ballantrae lavas from  
1072 rare-earth element distributions. *Scottish Journal of Geology* 13, 211-222.  
1073
- 1074 Lindsley, D.H., 1976. The crystal chemistry and structure of oxide minerals as exemplified by the  
1075 Fe-Ti oxides. In Rumble III D (Ed), *Rev Mineral* 3:L1-L60.  
1076
- 1077 Maaløe, S., 2005. The dunite bodies, websterite and orthopyroxenite dikes of the Leka Ophiolite  
1078 Complex, Norway. *Mineralogy and Petrology* 85, 163–204.  
1079
- 1080 MacDonald, R., Fettes, D. J., 2006. The tectonomagmatic evolution of Scotland. *Transactions of the*  
1081 *Royal Society of Edinburgh: Earth Sciences* 97, 213-295.  
1082
- 1083 Marchesi, C., González-Jiménez, J. M., Gervilla, F., Garrido, C. J., Griffin, W. L., O'Reilly, S. Y.,  
1084 Proenza, J. A., Pearson, N. J., 2010. In situ Re-Os isotopic analysis of platinum-group minerals  
1085 from the Mayari-Cristal ophiolitic massif (Mayari-Baracoa ophiolitic belt, eastern Cuba):  
1086 implications for the origin of Os isotope heterogeneities in podiform chromitites. *Contributions to*  
1087 *Mineralogy and Petrology* 161, 977-990.  
1088
- 1089 Matveev, S., Ballhaus, C., 2002. Role of water in the origin of podiform chromitite deposits. *Earth*  
1090 *and Planetary Science Letters* 203, 235-243.  
1091
- 1092 Maurel, C., Maurel, P., 1982. Etude expérimentale de la distribution de l'aluminium entre bain  
1093 silicaté basique et spinelle chromifère. Implications pétrogénétiques: teneur en chrome des  
1094 spinelles. *Bulletin de Minéralogie* 105, 197-202.  
1095
- 1096 Melcher, F., Grum, W., Simon, G., Thalhammer, T. V., Stumpfl, E. F., 1997. Petrogenesis of the  
1097 Ophiolitic Giant Chromite Deposits of Kempirsai, Kazakhstan: a study of solid and fluid inclusions  
1098 in chromite. *Journal of Petrology* 38, 1419-1458.  
1099
- 1100 Miller, C., Zanetti, A., Thöni, M., Konzett, J., Klötzli, U., 2012. Mafic and silica-rich glasses in  
1101 mantle xenoliths from Wau-en-Namus, Libya: textural and geochemical evidence for peridotite-  
1102 melt reactions. *Lithos* 128-131, 11-26.  
1103
- 1104 Morishita, T., Andal, E. S., Arai, S., Ishida, Y., 2006. Podiform chromitites in the Iherzolite-  
1105 dominant mantle section of the Isobela ophiolite, the Philippines. *Island Arc* 15, 84-101.  
1106
- 1107 Nestola, F., Ballaran, T. B., Balic-Zunic, T., Princivalle, F., Secco, L., Dal Negro, A., 2007.  
1108 Comparative compressibility and structural behaviour of spinel  $MgAl_2O_4$  at high pressures: the  
1109 independency on the degree of cation order. *American Mineralogist* 92, 1838-1843.  
1110

- 1111 O'Driscoll, B., Day, J. M. D., Walker, R. J., Daly, J. S., McDonough, W. F., Piccoli, P. M., 2012a.  
 1112 Chemical heterogeneity in the upper mantle recorded by peridotites and chromitites from the  
 1113 Shetland Ophiolite Complex, Scotland. *Earth and Planetary Science Letters* 333-334, 226-237.  
 1114
- 1115 O'Driscoll, B., Derbyshire, E.J., Gertisser, R., 2012b. Snapshots of ancient oceanic mantle captured  
 1116 in British and Irish ophiolites. *Geology Today*, 28(4), 134-140.  
 1117
- 1118 O'Driscoll, B., Walker, R.J., Day, J.M.D., Ash, R.D., Daly, J.S. 2015. Generations of melt  
 1119 extraction, melt-rock interaction and high-temperature metasomatism preserved in peridotites of the  
 1120 ~497 Ma Leka Ophiolite Complex, Norway. *Journal of Petrology*, 56(9), 1797-1828.  
 1121
- 1122 Oliver, G. J. H., McAlpine, R. R., 1998. Occurrence of a sheeted dyke complex in the Ballantrae  
 1123 ophiolite, Scotland. *Geological Magazine* 135, 509-517.  
 1124
- 1125 Oliver, G. J. H., Stone, P., Bluck, B. J., 2002. The Ballantrae Complex and Southern Uplands  
 1126 terrane, in: Trewin, N. H. (Ed.), *The Geology of Scotland* (2nd Edition). The Geological Society,  
 1127 London, pp. 167-200.  
 1128
- 1129 Orberger, B., Lorand, J-P., Girardeau, J., Mercier, J. C. C., Pitragool, S., 1995. Petrogenesis of  
 1130 ultramafic rocks and associated chromitites in the Nan Uttaradit ophiolite, northern Thailand. *Lithos*  
 1131 35, 153-182.  
 1132
- 1133 Pagé, P., Barnes, S-J., 2009. Using Trace Elements in Chromites to Constrain the Origin of  
 1134 Podiform Chromitites in the Thetford Mines Ophiolite, Québec, Canada. *Economic Geology* 104,  
 1135 997-1018.  
 1136
- 1137 Peach, B. M., Horne, J., 1899. *The Silurian rocks of Great Britain. Volume I, Scotland. Memoir of*  
 1138 *the Geological Survey of Great Britain* 18, pp. 1-749.  
 1139
- 1140 Piccardo, G. B., Zanetti, A., Muntener, O., 2007. Melt/peridotite interaction in the Southern Lanzo  
 1141 peridotite: Field, textural and geochemical evidence. *Lithos* 94, 181-209.  
 1142
- 1143 Power, M., Pirrie, D., 2004. Platinum-group minerals within the Ballantrae Complex, SW Scotland.  
 1144 *Scottish Journal of Geology* 40, 1-5.  
 1145
- 1146 Prichard, H. M., Lord, R. A., Neary, C. R., 1996. A model to explain the occurrence of Platinum-  
 1147 and Palladium-rich ophiolite complexes. *Journal of the Geological Society* 153, 323-328.  
 1148
- 1149 Prichard, H.M., Barnes, S.J., Godel, B., Reddy, S.M., Vukmanovic, Z., Halfpenny, A., Neary, C.R.,  
 1150 Fisher, P.C., 2015. The structure and origin of nodular chromite from the Troodos ophiolite, Cyprus,  
 1151 revealed using high-resolution X-ray computed tomography and electron backscatter diffraction.  
 1152 *Lithos* 218-219, 87-98.  
 1153
- 1154 Princivalle, F., Della Giusta, A., Carbonin, S., 1989. Comparative crystal chemistry of spinels from  
 1155 some suites of ultramafic rocks. *Mineralogy and Petrology* 40, 117- 126.  
 1156
- 1157 Princivalle, F., Della Giusta, A., De Min, A., Piccirillo, E. M., 1999. Crystal chemistry and  
 1158 significance of cation ordering in Mg-Al rich spinels from high-grade hornfels (Predazzo-Monzoni,  
 1159 NE Italy). *Mineralogical Magazine* 63, 257-262.  
 1160
- 1161 Pringle, J., 1935. *British Regional Geology: the south of Scotland*. HMSO, Edinburgh.  
 1162

1163 Rampone, E., Piccardo, G. B., Hofmann, A.W., 2008). Multi-stage melt-rock interaction in the Mt.  
1164 Maggiore (Corsica, France) ophiolitic peridotites: microstructural and geochemical evidence.  
1165 Contributions to Mineralogy and Petrology 156, 453-475.  
1166  
1167 Rollinson, H., 2005. Chromite in the mantle section of the Oman ophiolite: a genetic model. The  
1168 Island Arc 14, 542-550.  
1169  
1170 Rollinson, H., 2008. The geochemistry of mantle chromites from the northern part of the Oman  
1171 ophiolite: inferred parental melt compositions. Contributions to Mineral Petrology 156, 273-288.  
1172  
1173 Rollinson, H., Adetunji, J., 2013. Mantle podiform chromitites do not form beneath midocean  
1174 ridges: a case study from the Moho transition zone of the Oman ophiolite. Lithos 177, 314-327.  
1175  
1176 Ryan, P. D., Dewey, J. F., 1991. A geological and tectonic cross-section of the Caledonides of  
1177 western Ireland. Journal of the Geological Society 148, 173-180.  
1178  
1179 Sack, R. O., Ghirso, M. S., 1991. Chromium spinels as petrogenetic indicators: thermodynamics  
1180 and petrological applications. American Mineralogist 76, 827-847.  
1181  
1182 Sheldrick, G. M., 1997. SHELX-97 Program for crystal structure refinement. University of  
1183 Göttingen, Germany.  
1184  
1185 Smellie, J. L., Stone, P., 1992. Geochemical control on the evolutionary history of the Ballantrae  
1186 Complex, SW Scotland, from comparisons with recent analogues, in: Parson, L. M., Murton, B.J.,  
1187 Browning, P. (Eds.), Ophiolites and their Modern Analogues. Geological Society of London,  
1188 Special Publications 60, 171-178.  
1189  
1190 Smellie, J. L., Stone, P., 2001. Geochemical characteristics and geotectonic setting of early  
1191 Ordovician basalt lavas in the Ballantrae Complex ophiolite, SW Scotland. Transactions of the  
1192 Royal Society of Edinburgh: Earth Sciences 91, 539-555.  
1193  
1194 Smellie, J. L., Stone, P., Evans, J., 1995. Petrogenesis of boninites in the Ordovician Ballantrae  
1195 Complex ophiolite, southwestern Scotland. Journal of Volcanology and Geothermal Research 69,  
1196 323-342.  
1197  
1198 Stone, P., Smellie, J. L., 1988. *The Ballantrae area: a description of the solid geology of parts of*  
1199 *1:25 000 sheets NX08, 18 and 19.* Classical areas of British Geology. HMSO for British Geological  
1200 Survey.  
1201  
1202 Stone, P., 2014. A review of geological origins and relationships in the Ballantrae Complex, SW  
1203 Scotland. Scottish Journal of Geology 50(1), 1-25.  
1204  
1205 Strachan, R. A., Smith, M., Harris, A. L., Fettes, D. J., 2002. The Northern Highland and Grampian  
1206 terranes, in: Trewin, N. H. (Ed.), The Geology of Scotland. The Geological Society, London, pp.  
1207 167-200.  
1208  
1209 Thirlwall, M. F., Bluck, B. J., 1984. Sr-Nd isotope and chemical evidence that the Ballantrae  
1210 'ophiolite', SW Scotland, is polygenetic, in: Gass, I. G., Lippard, S. J., Shelton, A. W. (Eds.),  
1211 Ophiolites and Oceanic Lithosphere, Geological Society of London Special Publications 13, 215-  
1212 230.  
1213

- 1214 Uchida, H., Lavina, B., Downs, R. T., Chesley, J., 2005. Single-crystal X-ray diffraction of spinels  
1215 from the San Carlos Volcanic Field, Arizona: spinel as a geothermometer. *American Mineralogist*  
1216 90, 1900-1908.  
1217
- 1218 Uysal, I., Tarkian, M., Burhan Sadilar, M., Zaccarini, F., Meisel, T., Garuti, G., Heidrich, S., 2009.  
1219 Petrology of Al- and Cr-rich ophiolitic chromitites from the Mugla, SW Turkey: implications from  
1220 composition of chromite, solid inclusions of platinum group mineral, silicate, and base-metal  
1221 Contributions to Mineralogy and Petrology 158, 659-674.  
1222
- 1223 Voigt, M., von der Handt, A., 2011. Influence of subsolidus processes on the chromium number in  
1224 spinel in ultramafic rocks. *Contributions to Mineralogy and Petrology* 162, 675-689.  
1225
- 1226 Vuollo, J., Liipo, J., Nykänen, V., Piirainen, T., Pekkarinen, L., Tuokko, I., Ekdahl, E., 1995. An  
1227 early Proterozoic podiform chromitite in the Outokumpu Ophiolite Complex, Finland. *Economic*  
1228 *Geology* 90, 445-452.  
1229
- 1230 Whattam, S. A., Stern, R. J., 2011. The 'subduction initiation rule': a key for linking ophiolites,  
1231 intra-oceanic forearcs, and subduction initiation. *Contributions to Mineralogy and Petrology* 162,  
1232 1031-1045.  
1233
- 1234 Wilkinson, J. M., Cann, J. R., 1974. Trace elements and tectonic relationships of basaltic rocks in  
1235 the Ballantrae igneous complex, Ayrshire. *Geological Magazine* 111, 35- 41.  
1236
- 1237 Xiong, F., Yang, J., Robinson, P.T., Xu, X., Liu, Z., Zhou, W., Feng, G., Xu, J., Li, J. and Niu, X.  
1238 2017. High-Al and high-Cr podiform chromitites from the western Yarlung-Zangbo suture zone,  
1239 Tibet: Implications from mineralogy and geochemistry of chromian spinel, and platinum-group  
1240 elements. *Ore Geology Reviews* 80, 1020-1041.  
1241
- 1242 Zagrtdenov, NR, Ceuleneer, G., Rospabé, M., Borisova, AY., Toplis, MJ., Benoit, M. and Abily, B.  
1243 2018. Anatomy of a chromitite dyke in the mantle/crust transition zone of the Oman ophiolite.  
1244 *Lithos* 312-313, 343-357.  
1245
- 1246 Zhou, M-F., Robinson, P. T., 1997. Origin and tectonic environment of podiform chromite deposits.  
1247 *Economic Geology* 92, 259-262.  
1248
- 1249 Zhou, M-F., Robinson, P. T., Malpas, J., Li, Z., 1996. Podiform chromites in the Luobusa Ophiolite  
1250 (Southern Tibet): Implications for melt-rock interaction and chromite segregation in the upper  
1251 mantle. *Journal of Petrology* 37, 3-21.  
1252
- 1253 Zhou, M-F., Malpas, J., Robinson, P. T., Sun, M., Li, J-W., 2001. Crystallisation of podiform  
1254 chromitites from silicate magmas and the formation of nodular textures. *Resource Geology* 51, 1-6.  
1255  
1256  
1257  
1258  
1259  
1260  
1261  
1262  
1263  
1264  
1265

1266 **Figure Captions**

1267

1268 **Figure 1.** Geological sketch map of the Ballantrae Ophiolite Complex, Scotland, showing the major  
1269 lithological units and the locations of the Pinbain Bridge and Poundland Burn chromitite bodies.  
1270 The sketch map is adapted from those in Stone (2014). The inset is a regional map of Scotland  
1271 showing the regional location of the BOC in Ayrshire (red square).  
1272

1273 **Figure 2.** (a) Field photograph illustrating typical harzburgite texture at Pinbain Bridge. (b) Nodular  
1274 chromitite at Poundland Burn; the nodules are up to 1 cm in diameter and are hosted in a  
1275 serpentinised dunite matrix. (c) Anti-nodular chromitite in close proximity to (b). The silicate  
1276 nodules comprise serpentinite and are <1 cm in size, with a groundmass network of fine-grained Cr-  
1277 spinel crystals. Pen-tip is shown for scale in (a) – (c).  
1278

1279 **Figure 3.** (a-b) Backscattered electron micrographs of chromitite textures from Pinbain Bridge.  
1280 Note the thin discontinuous Fe-rich (bright) rim on the grey Cr-spinel crystal in (a) and the fracture  
1281 and associated brittle deformation in chromitite in (b). In (a) and (b), the black-coloured  
1282 groundmass is predominantly serpentinite. (c) Thin section scan of BA-10-06 nodular-textured  
1283 chromitite. The cusped-shaped areas infilled with silicate in nodule centres (located within the red  
1284 outline in one nodule) and relatively massive outer nodule mantles are described in the text. (d)  
1285 Plane polarised light photomicrograph of orthopyroxene pseudomorph in a serpentinised  
1286 harzburgite from Poundland Burn, in which bastite is partly replacing orthopyroxene. (e) Plane  
1287 polarised light photomicrograph of Poundland Burn dunite – note the elongate stringer of Cr-spinel  
1288 crystals (black) in the bottom-right of the image, as well as other isolated Cr-spinel crystals  
1289 elsewhere in the serpentinised olivine groundmass. (f) Backscattered electron micrograph of  
1290 accessory Cr-spinel from Poundland Burn dunite, with relatively thick Fe-rich rim and abundant  
1291 silicate inclusions.  
1292

1293 **Figure 4.** Panels illustrate the internal structure and chemical composition of a single Cr-spinel  
1294 nodule from Poundland Burn (Sample BA-10-06). (a) Thin section scan showing the location (red  
1295 square) of the nodule featured in (b) and (c). (b) Mineral chemical transect of the nodule, showing  
1296 the relative homogeneity in Mg#, Cr# and TiO<sub>2</sub> from one side to the other. The transect represents  
1297 40 individual spot points, from X-Y, taken at equal spacings apart on the traverse shown in (c), but  
1298 avoiding inclusions and fractures. (c) Stitched backscattered electron micrographs, showing the  
1299 internal structure of an individual nodule and the position of the electron microprobe traverse shown  
1300 in (b).  
1301

1302 **Figure 5.** Plots of (a) Cr# versus Mg# and (b) TiO<sub>2</sub> versus Cr# discriminate the tectonic setting (and  
1303 parental melt composition) of the Ballantrae Cr-spinels. In (a), the two solid black outline ellipses  
1304 delineate the range of Pinbain Bridge and Poundland Burn chromitite compositions. The fields for  
1305 boninite and abyssal peridotite are taken from Dick and Bullen (1984) and Kepezhinskis et al.  
1306 (1993). The green field is the range of peridotite accessory Cr-spinel compositions referred to in  
1307 Dare et al. (2009); it is important to note that the Ballantrae chromitite Cr-spinels fall outside of the  
1308 outer limits of this field. In (b), the fields for MORB/boninite and layered intrusions, ophiolites and  
1309 komatiites, come from Hunt et al. (2012) and references therein.  
1310

1311 **Figure 6.** Trace element characteristics of the Ballantrae Cr-spinels. (a) V versus Cr#, (b) Co versus  
1312 Cr#, (c) Ga versus Cr# and (d) Cu/Zn versus Cu/Ni. The symbols are the same as in **Figure 5**.  
1313 Ranges of trace element compositions for the Lizard, Shetland and Corrycharmaig are shown for  
1314 comparison (B O'Driscoll; unpublished data). The MORB and two boninite compositions come  
1315 from Pagé and Barnes (2009). The symbols are the same as for **Figure 5**, unless otherwise  
1316 specified. In (d), the R<sup>2</sup> values were calculated by least squares regression in Microsoft Excel.  
1317

1318 **Figure 7.** Spidergram showing the major and trace element characteristics of the Ballantrae Cr-  
1319 spinels, relative to two boninite compositions, and normalised to MORB. The boninite and MORB  
1320 compositions are taken from Pagé and Barnes (2009). Abbreviations as follows: TMO, Thetford  
1321 Mines Ophiolite; EPR, East Pacific Rise. See text for further discussion.  
1322

1323 **Figure 8.** (a) Crystal structural analysis plot displaying cell edge length ( $a_0$ ) against oxygen  
1324 positional parameter ( $u$ ). The majority of the Ballantrae Cr-spinels have low  $a_0$  and higher  $u$  values  
1325 than the Shetland Ophiolite Complex Cr-spinels (orange field) from Derbyshire et al. (2013). (b)  
1326 Cr-spinel crystal structural plot displaying Cr# versus oxygen positional parameter ( $u$ ). The Pinbain  
1327 Bridge Cr-spinels have higher Cr contents and correspondingly smaller  $u$  values whilst the  
1328 Poundland Burn Cr-spinels display relatively consistent Cr contents across a small range in  $u$   
1329 (0.2629-0.2634). The symbols are the same as for **Figure 5**, unless otherwise specified.  
1330

1331 **Figure 9.** (a) The Ti/Fe<sup>3</sup># versus Ga/Fe<sup>3</sup># diagram of Dare et al. (2009), illustrating that the  
1332 Ballantrae Cr-spinels, in particular those from the Poundland Burn dunites, have compositions  
1333 spanning the boundary between MOR-reacted and SSZ-reacted compositions (though mainly in the  
1334 latter). Chromitite compositions are plotted too for reference but these are probably unreliable for  
1335 the reasons outlined in Dare et al. (2009). The ranges of compositions of Shetland, Lizard and  
1336 Corrycharmaig Cr-spinels are also shown for comparison, and it is notable that the Lizard Cr-  
1337 spinels in particular, which are an accessory phase in dunite, plot in the MOR-reacted field,  
1338 consistent with published interpretations of the Lizard as a MORB-type ophiolite (O'Driscoll et al.  
1339 2012b). (b) Calculated TiO<sub>2</sub> versus Al<sub>2</sub>O<sub>3</sub> for the Ballantrae Cr-spinel parental melts. See text for  
1340 further discussion. The values for MORB and boninite, as well as the various boninite fields, come  
1341 from Pagé and Barnes (2009). The grey-shaded boninite and MORB fields come from Rollinson  
1342 (2008). The symbols are the same as for **Figure 5**, unless otherwise specified.  
1343  
1344  
1345  
1346  
1347  
1348  
1349  
1350  
1351  
1352  
1353  
1354  
1355  
1356  
1357  
1358  
1359  
1360  
1361  
1362  
1363  
1364  
1365  
1366  
1367  
1368  
1369



Sample	BA-10-03	BA-10-04	BA-10-06	BA-10-07	BA-10-10	BA-10-11	BA-10-12	BA-10-13
$a_0$	8.27043 (9)	8.2740 (4)	8.2206 (3)	8.2204 (3)	8.2205 (1)	8.2456 (4)	8.2528 (3)	8.2285 (5)
$u$	0.2625 (1)	0.2627 (1)	0.2630 (1)	0.2630 (1)	0.2631 (1)	0.2631 (1)	0.2629 (1)	0.2634 (2)
MgO	14.5 (2)	15.2 (2)	16.8 (3)	16.8 (3)	16.7 (2)	13.5 (3)	13.3 (2)	15.6 (3)
Al <sub>2</sub> O <sub>3</sub>	18.3 (2)	19.9 (4)	30.9 (4)	30.9 (2)	30.7 (4)	27.0 (5)	26.3 (5)	29.0 (1)
TiO <sub>2</sub>	0.12 (2)	0.11 (1)	0.26 (1)	0.24 (2)	0.28 (2)	0.25 (2)	0.26 (2)	0.24 (2)
Cr <sub>2</sub> O <sub>3</sub>	50.4 (2)	49.3 (3)	37.4 (3)	37.5 (4)	37.6 (3)	34.3 (4)	33.7 (6)	36.8 (5)
MnO	0.21 (3)	0.21 (4)	0.18 (3)	0.18 (3)	0.19 (3)	0.25 (2)	0.24 (3)	0.19 (3)
FeO <sub>tot</sub>	16.1 (2)	14.8 (1)	14.0 (2)	13.9 (2)	14.2 (1)	23.5 (7)	25.1 (4)	17.4 (2)
NiO	0.10 (3)	0.17 (4)	0.20 (1)	0.18 (4)	0.18 (4)	0.20 (3)	0.24 (2)	0.18 (3)
ZnO*	0.07 (2)		0.07 (2)		0.05 (2)	0.14 (3)	0.17 (3)	
<b>Sum</b>	99.84	99.74	99.84	99.65	99.88	99.25	99.27	99.41
FeO	12.6 (2)	11.6 (1)	11.0 (2)	11.1 (2)	11.3 (1)	15.2 (7)	15.4 (4)	12.6 (2)
Fe <sub>2</sub> O <sub>3</sub>	3.96	3.61	3.33	3.13	3.21	9.25	10.8	5.36
<b>Sum</b>	100.24	100.10	100.17	99.96	100.20	100.18	100.35	99.95
<b>T site</b>								
Mg	0.639 (7)	0.672 (8)	0.683 (9)	0.66 (1)	0.663 (8)	0.55 (1)	0.540 (9)	0.639 (9)
Al	0.027 (1)	0.026 (2)	0.029 (2)	0.042 (2)	0.028 (2)	0.025 (2)	0.032 (2)	0.015 (1)
Mn	0.006 (1)	0.006 (1)	0.004 (1)	0.004 (1)	0.005 (1)	0.006 (1)	0.006 (1)	0.005 (1)
Fe <sup>2+</sup>	0.295 (4)	0.297 (4)	0.242 (4)	0.263 (5)	0.267 (4)	0.38 (1)	0.379 (9)	0.311 (5)
Fe <sup>3+</sup>	0.032 (4)		0.040 (6)	0.034 (7)	0.036 (5)	0.040 (7)	0.040 (4)	0.030 (4)
Zn	0.002 (1)		0.002 (1)		0.001 (1)	0.003 (1)	0.004 (1)	
<b>M site</b>								
Mg	0.028 (2)	0.027 (2)	0.044 (2)	0.070 (4)	0.058 (2)	0.057 (4)	0.059 (3)	0.042 (2)
Al	0.643 (6)	0.68 (1)	1.03 (1)	1.020 (8)	1.030 (9)	0.94 (1)	0.91 (1)	0.998 (7)
Ti	0.003 (1)	0.003 (1)	0.006 (1)	0.005 (1)	0.006 (1)	0.006 (1)	0.006 (1)	0.005 (1)
Cr	1.234 (6)	1.195 (9)	0.858 (8)	0.862 (9)	0.861 (7)	0.81 (1)	0.81 (1)	0.861 (9)
Fe <sup>2+</sup>	0.028 (1)	0.002 (1)	0.024 (1)	0.006 (1)	0.007 (1)	0.007 (2)	0.013 (2)	
Fe <sup>3+</sup>	0.061 (5)	0.086 (8)	0.031 (6)	0.033 (7)	0.034 (5)	0.17 (1)	0.20 (1)	0.089 (7)
Ni	0.003 (1)	0.004 (1)	0.005 (1)	0.004 (1)	0.004 (1)	0.005 (1)	0.006 (1)	0.004 (1)
F(X)	0.23	0.27	0.09	0.05	0.14	0.21	0.05	0.20
T°C	853	793	623	708	630	724	789	591

1372  
1373  
1374  
1375  
1376  
1377  
1378  
1379  
1380  
1381

**Table 1.** Cell parameters, chemical analyses and cation distribution of Cr-spinels analysed by X-ray single crystal diffraction. Mean chemical analyses (up to 15 spot analyses for each crystal) and cation distribution in T and M site of the analyzed Cr-spinels on the basis of four oxygen atoms per formula unit. Fe<sup>3+</sup> from stoichiometry.  $a_0$ : cell parameter (Å);  $u$ : oxygen positional parameter; F(x): minimization factor, which takes into account the mean of square differences between calculated and observed parameters, divided by their standard deviations. Estimated standard deviations are in brackets. Intracrystalline closure temperature calculated by using the Princivalle et al (1999) thermometer. \*Zinc distribution is not reported when the standard deviation on chemistry is higher than the half of the mean value.

Figure 1

Figure 1

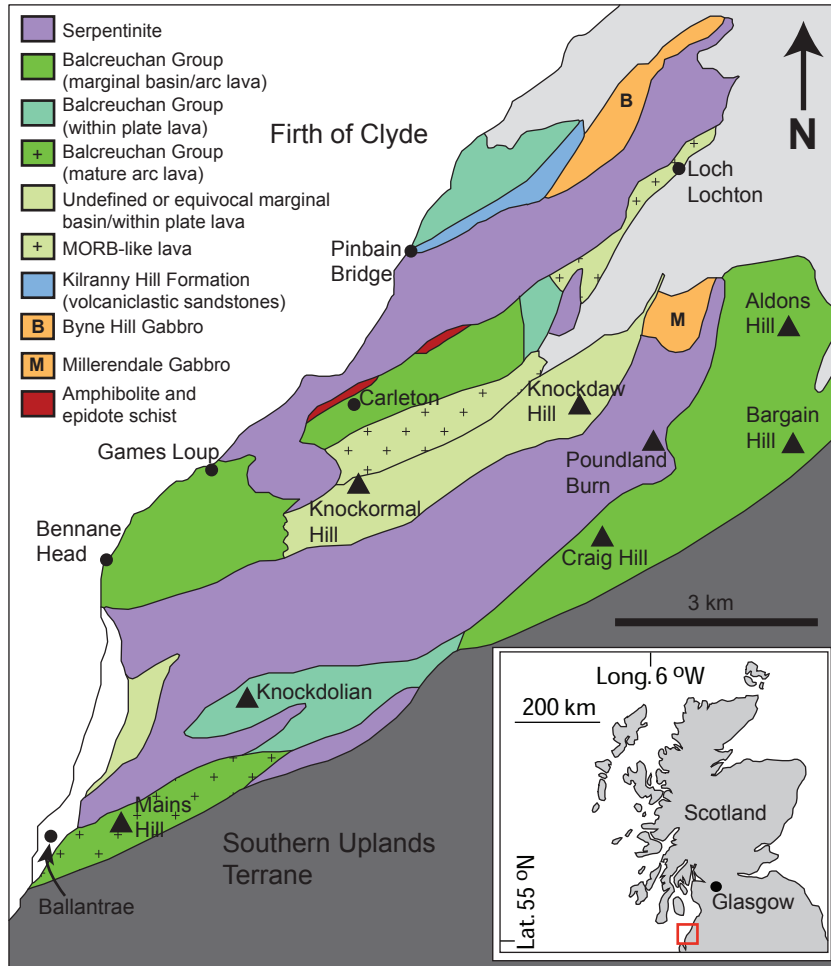


Figure 2

Figure 2

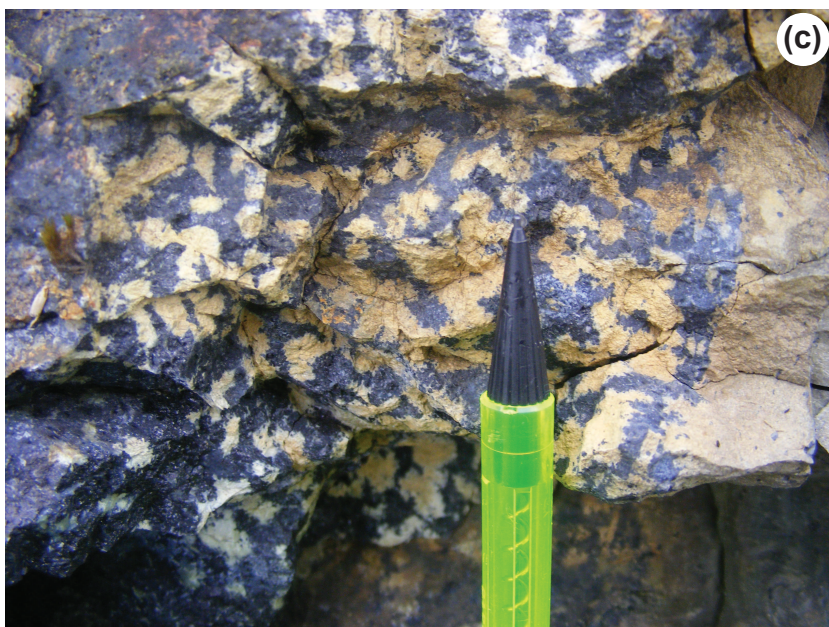
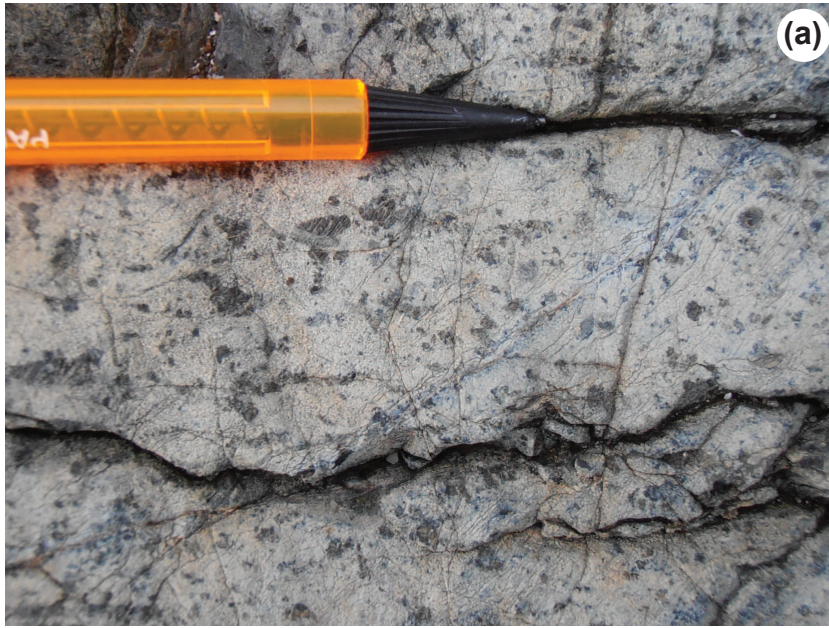


Figure 3

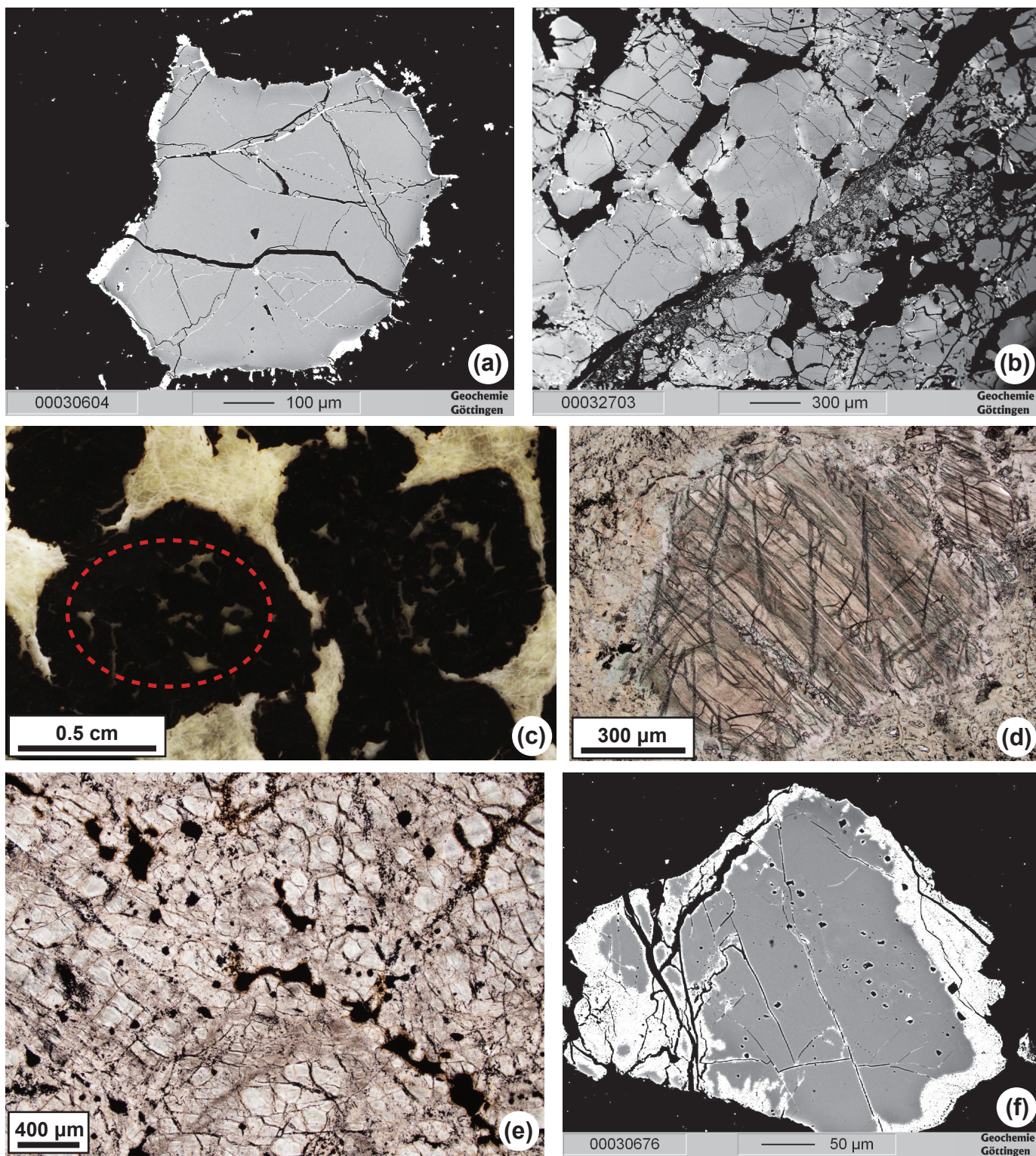


Figure 4

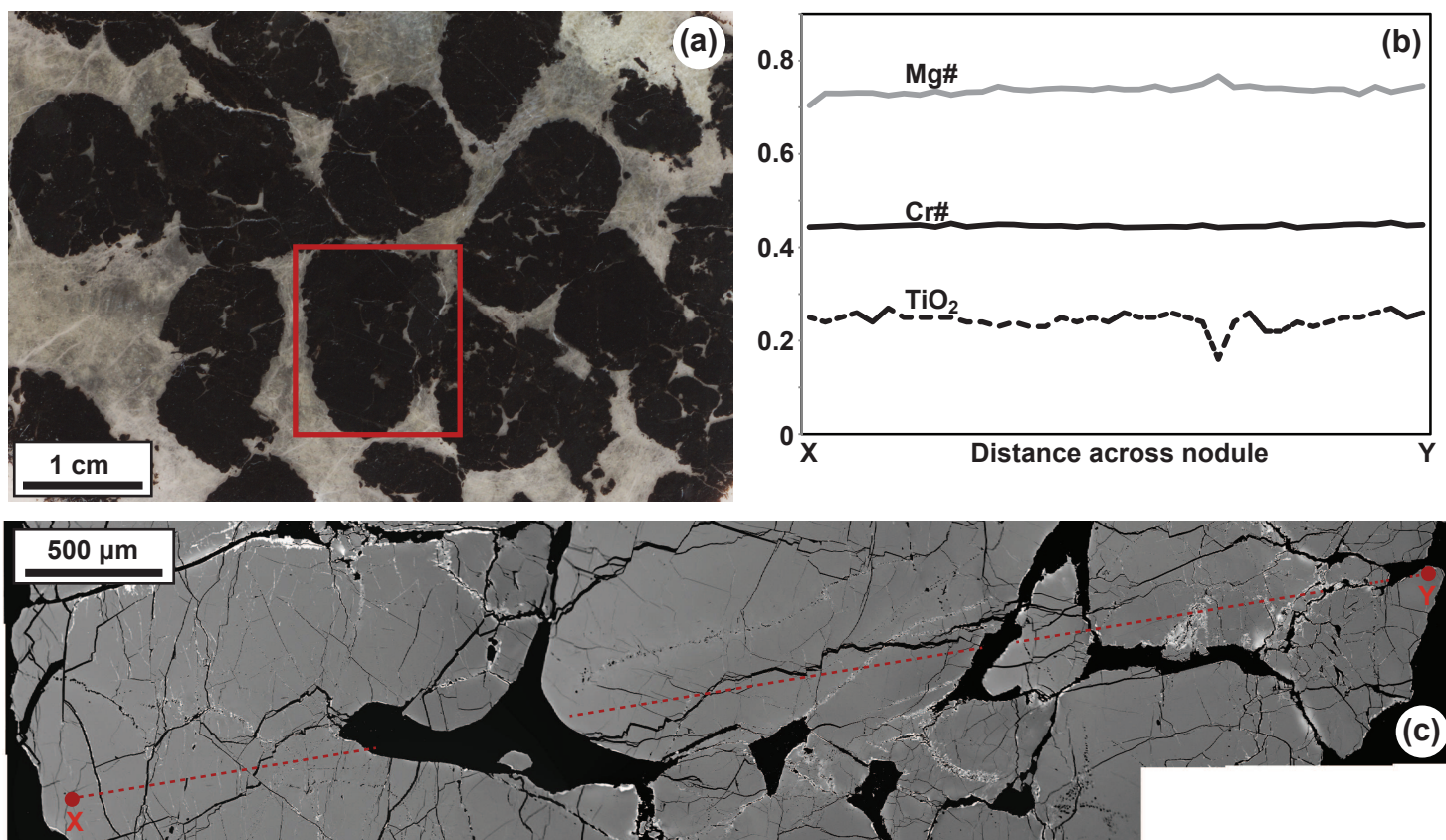


Figure 5

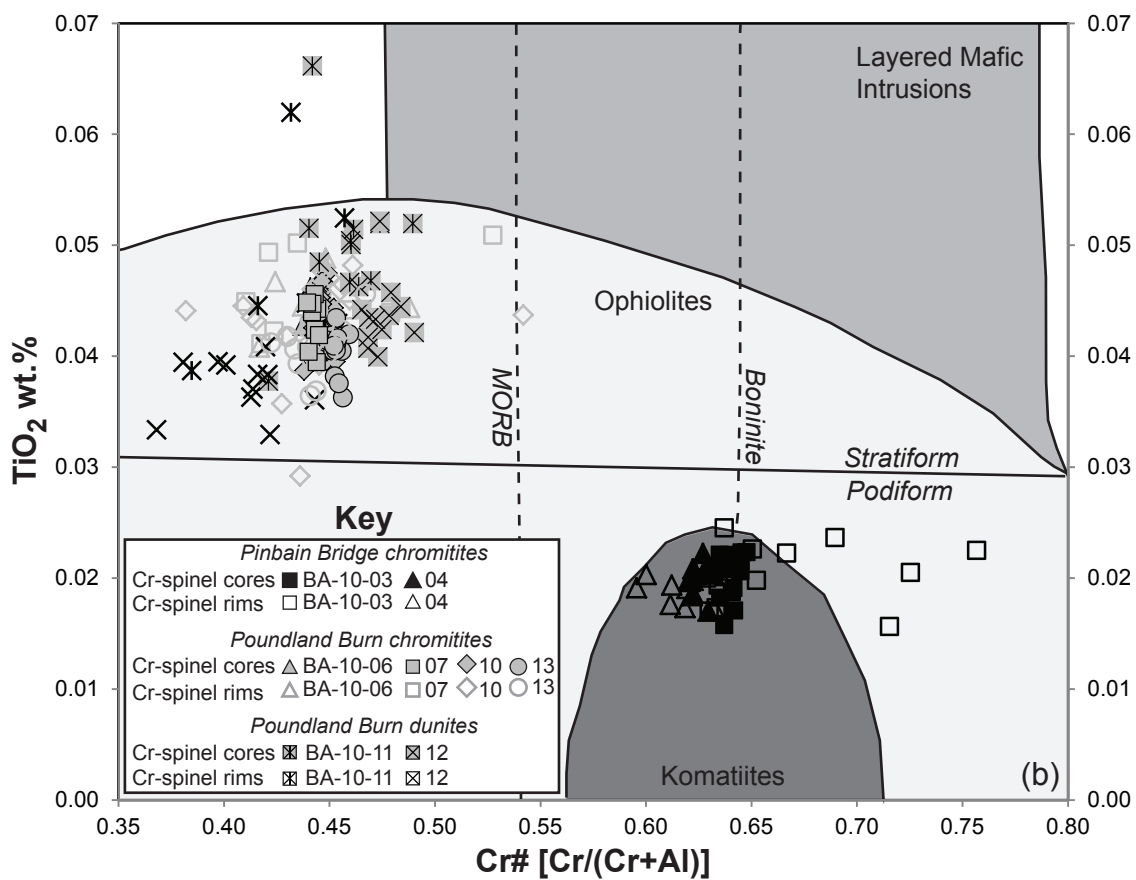
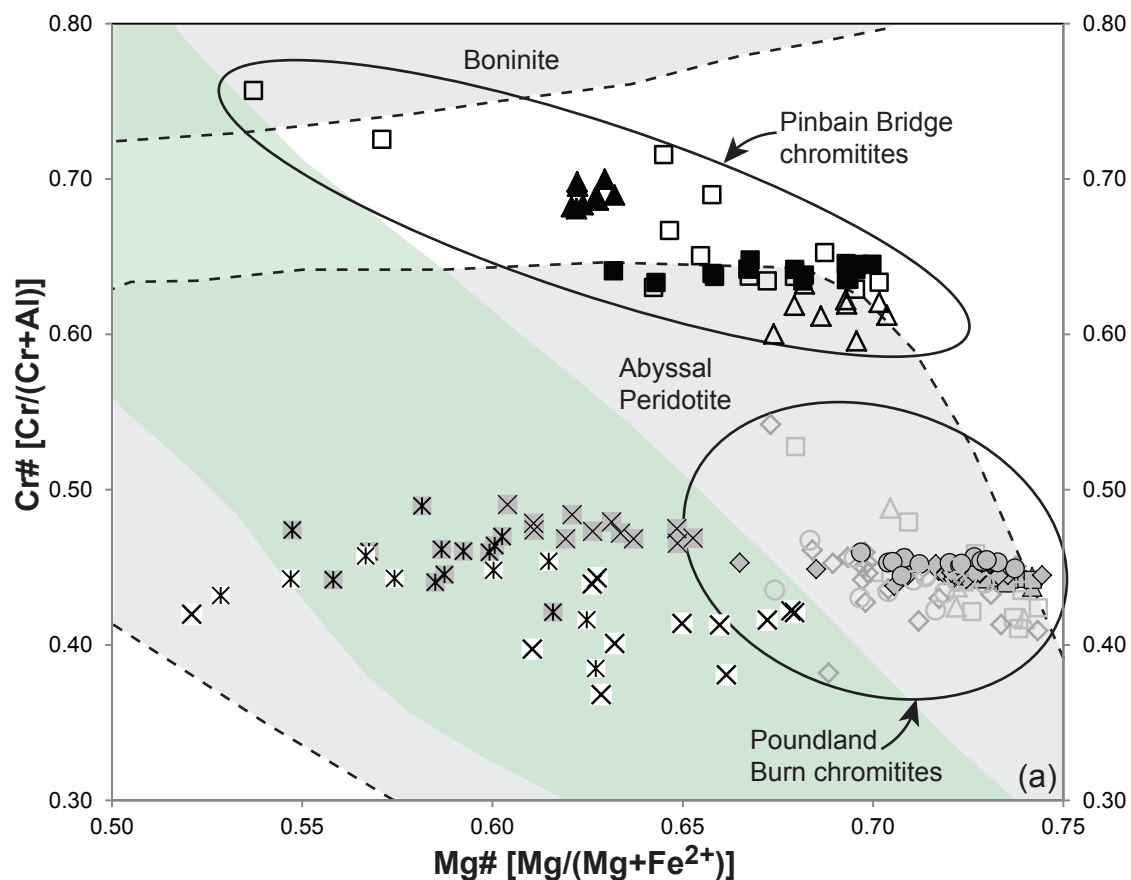


Figure 6

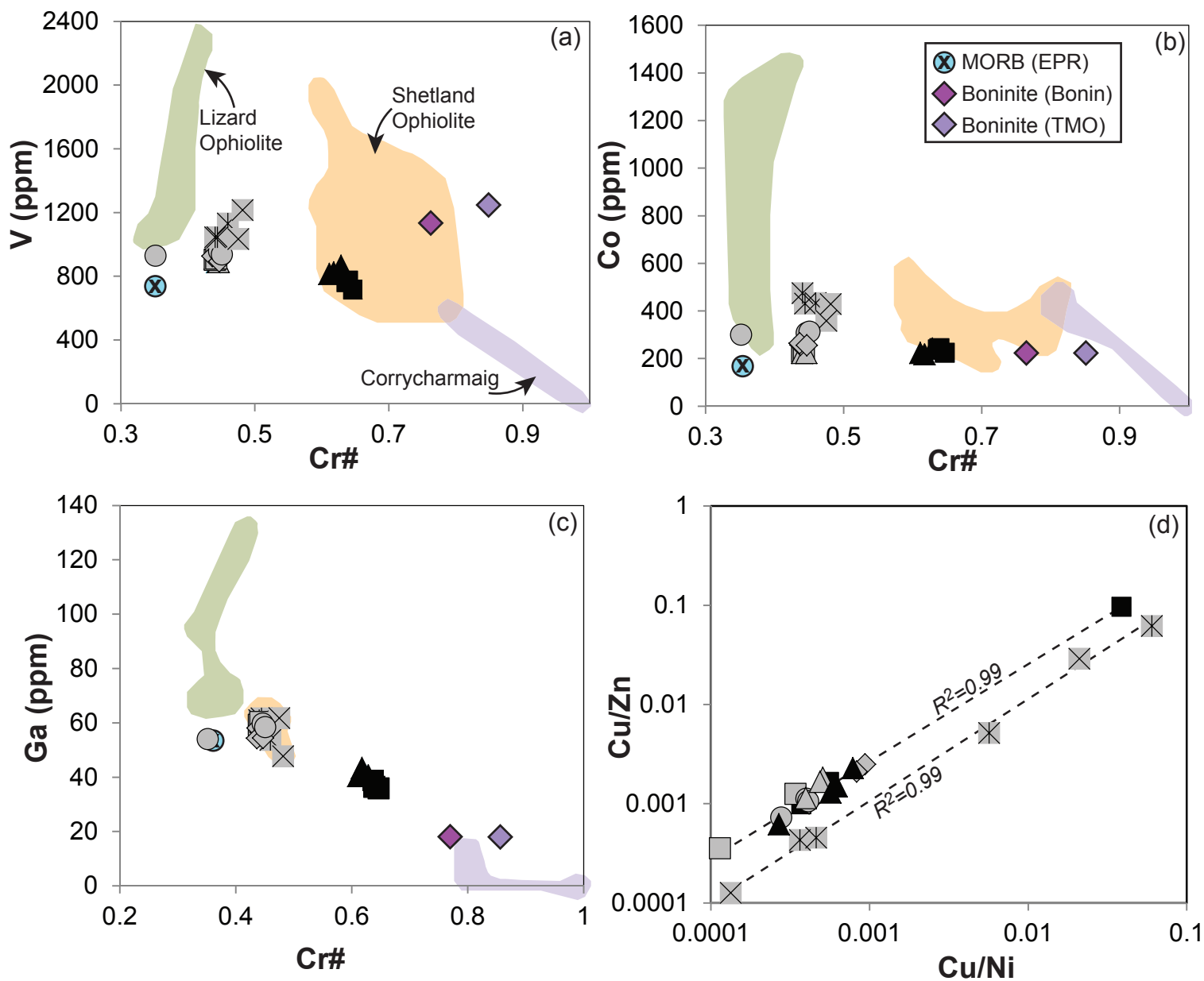


Figure 7

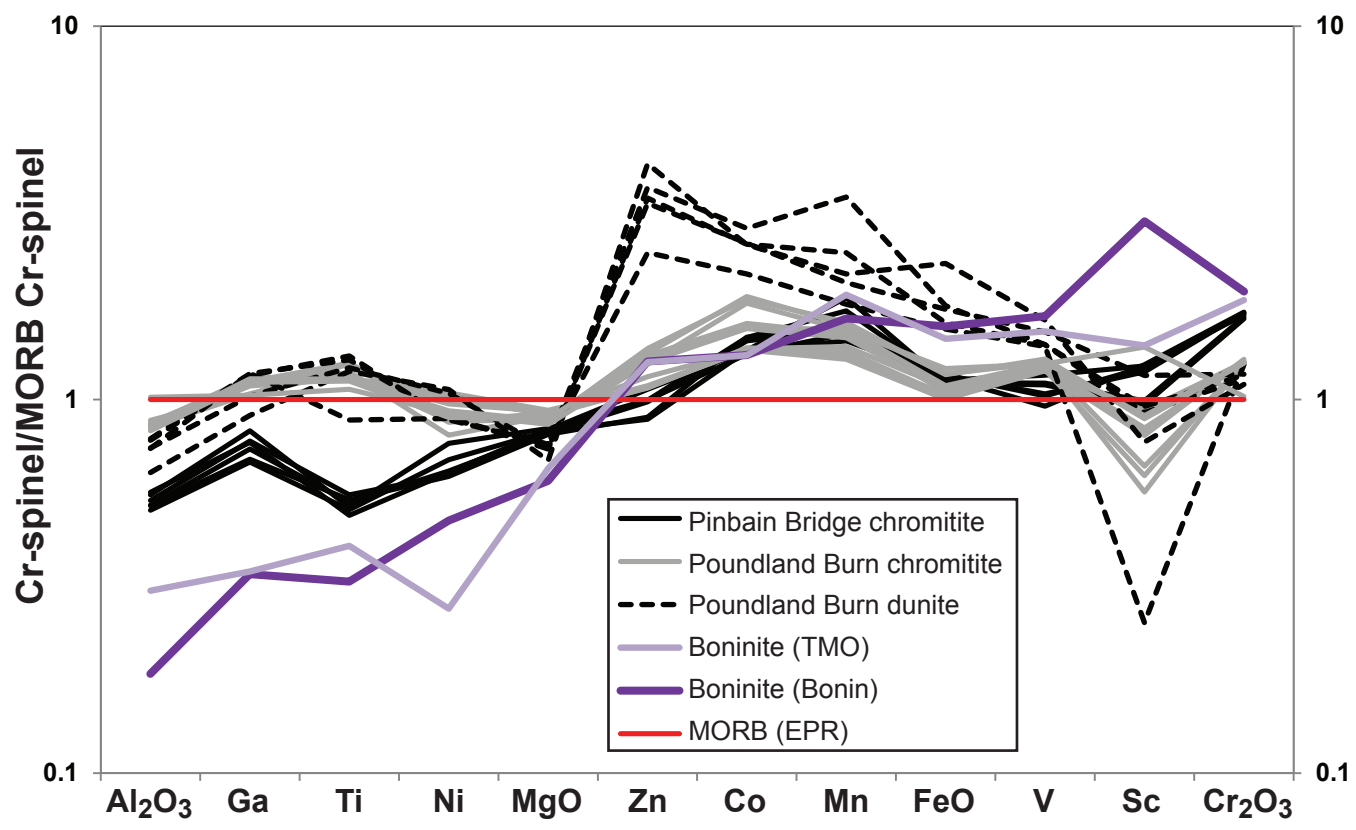




Figure 8

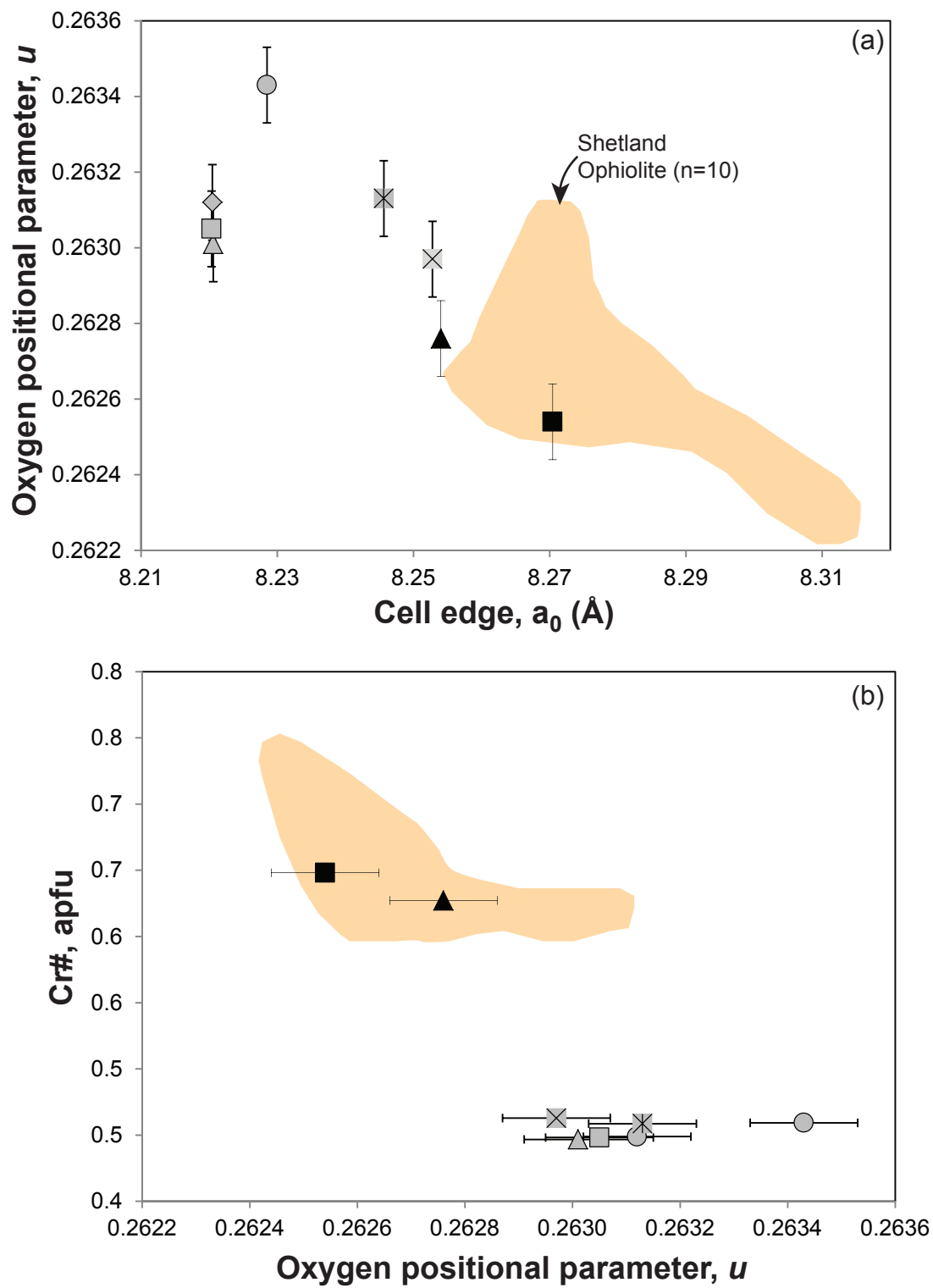
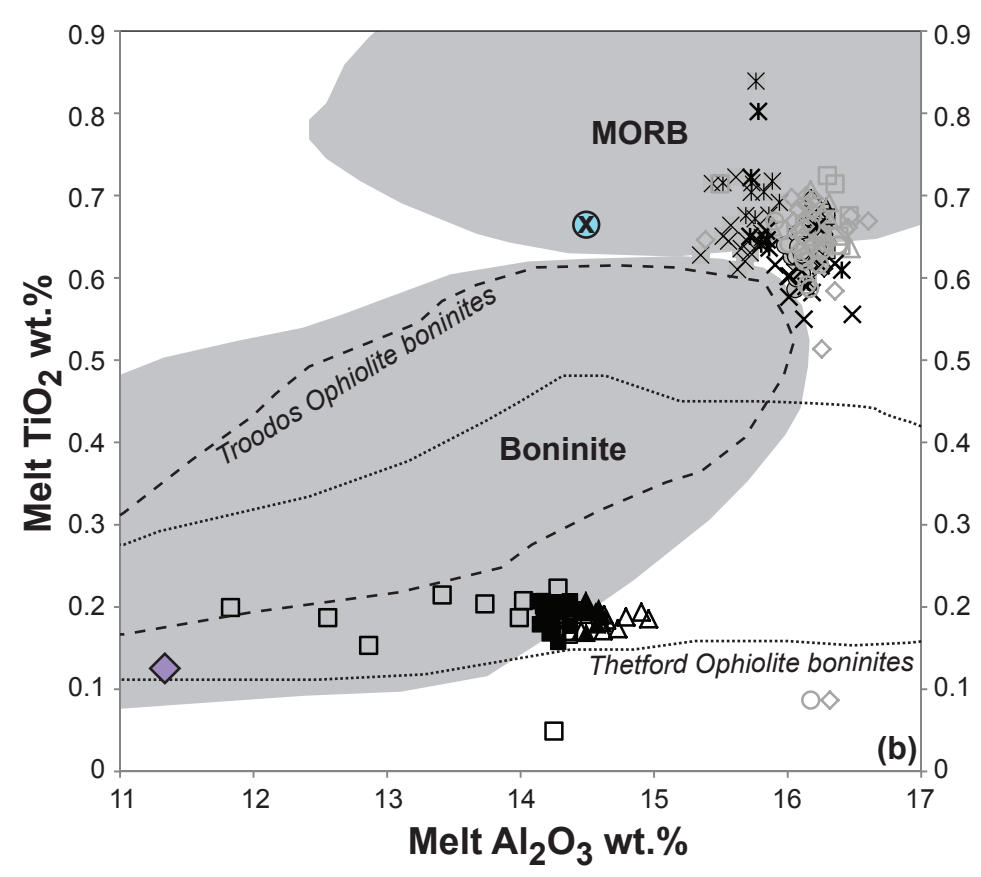
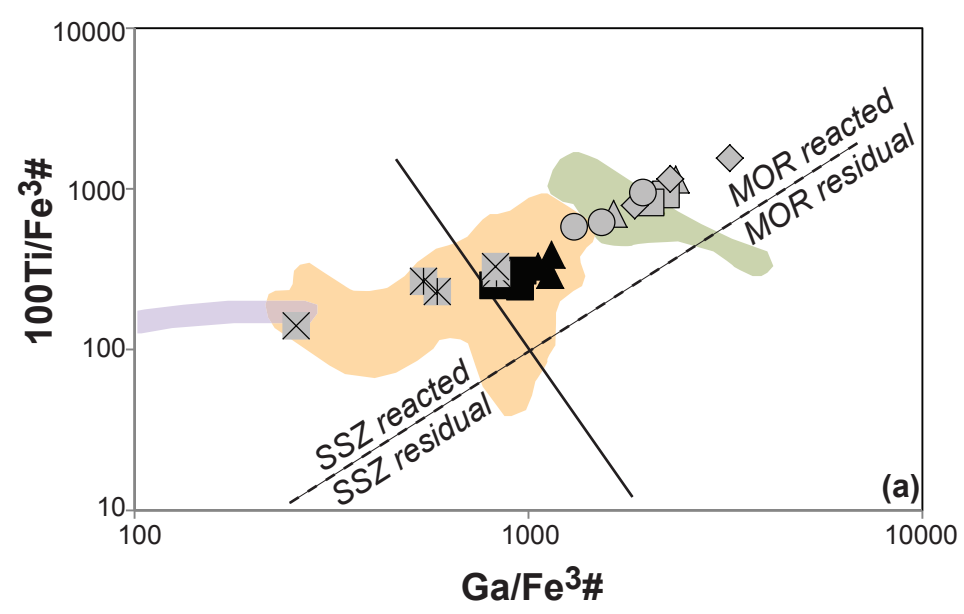


Figure 9



**Supplementary Tables S1,S2**

[Click here to download Background dataset for online publication only: Supplementary Tables S1,S2.xls](#)